Republic of Iraq
Ministry of Higher Education
And Scientific Research
University of Babylon
College of Materials Engineering
Department of Metallurgical Engineering

Multi- Optimization of sol-gel coating on low carbon steel for corrosion protection

A Thesis

Submitted to College of Materials Engineering of the University of Babylon in Partial Fulfillment of the Requirements for the Degree of Master in Materials Engineering / Metallurgy

By

Ammar Hussein Ali Hussein

(B.Sc. In Materials Engineering)

(2015)

Supervised by

Prof.Dr. Ekbal M.S. Salih

Prof.Dr. Haydar A.H. Al- juboori

1443 A.H **2022 A.D.**

بِسْمِ اللَّهِ الرَّحْمَنِ الرَّحِيمِ

۞ وَيَسئلُونَكَ عَنِ الرُّوحِ قُلِ الرُّوحُ مِنْ
أَمْرِ رَبِّي وَمَا أُوتِيتُم مِّن الْعِلْمِ إِلاَّ قَلِيلاً ۞

صدق الله العلي العظيم

{ سورة الإسراء / آية 85}

Supervisors Certificate

We certify that this thesis entitled **" Optimal protection for chemical industrial parts "- case Study"** is prepared by

(Ammar Hussein Ali AL-Shammari)

Under our supervision at the Department of Metallurgical Engineering/ College of Materials Engineering/ University of Babylon in partial fulfillment of the requirements for the Degree of Master in Material's Engineering/Metallurgical.

Signature:

Name of Supervisor:

Prof.Dr. Haydar A.H. Al- juboori

Date: / / 2022

Signature:

Name of Supervisor:

Prof. Dr. Ekbal M.S. Salih

Date: / / 2022

Dedications

To:

my mother

My father

My wife and children

My sister and

brothers

With love and respect

AMMAR AL-SHAMMARI

"Acknowledgement"

First of all, I would like to give much appreciation to God, who helped me to accomplish this work . want to express my appreciation to my supervisors, Prof. Dr. Haider Abdul Hassan Al-Jubouri and Dr. Iqbal Muhammad Saeed Saleh, for the excitement and support they have given me. This mission could not have been completed without their invaluable recommendations, guidance, and spiritual support during difficult times. My Friend Alaa Hussein, who has a Ph.D., was a tremendous help, and I am grateful to him. In addition, I would like to express my gratitude to both the Department of Metallurgical Engineering and my college, Materials Engineering, for their assistance and excellent facilities. In conclusion, I would like to express my gratitude to the Babylon University Workshop Materials Laboratory team members

AMMAR AL- SHAMMARI

Abstract

It is known that applying coatings on metals is one of the most effective ways to protect the metal from the effects of the surrounding environment. Titanium oxide (TiO_2) and aluminum oxide (Al_2O_3) were used in this study due to their unique properties as coating materials and prepared with Sol-Gel technology and by method dip coated. The coating was carried out to protect the tubes from concentrated sulfuric acid (98%). The coating depends on the design of the experiments by response surface approach. Variables are temperature , the number of layers applied, and the amount of alumina added were the main factors that were changed during the experiment. The tests were verified by X-ray diffraction (XRD), scanning electron microscopy (SEM) , roughness (AFM), and corrosion tests performed in a medium containing 98% acid and light microscopy. The success of this study depends on creating the ideal model for the best heat treatment, number of layers, and percentage of alumina addition. This is necessary for the success of the search. It was discovered that the temperature of 588˚C, several layers equal to 2, and the percentage of adding alumina equal to 10% gave the best results regarding acid resistance. According to the results, the hardness value of the material increased from 2.1 to 8.2 GPa when exposed to these conditions, and the adhesion strength value was 32.8 MPa when measured at the maximum. In addition, the corrosion rate value decreased to 0.036 mm /y, and the erosion-corrosion decreased to $3.1 * 10^{-5}$ (g/cm^2 day). The corrosion rate and erosion-corrosion value are improved by 98% and 99%. Each of these values has been reduced from its original values. According to the corrosion test results, this coating is suitable for use with concentration a sulfuric acid of 98%.

List of Contents

Subjects		Pag.NO
Abstract		I
List of contents		IV
List of figures		VII
List of tables		XI
List of symbols and abbreviations		XII
	Chapter One Introduction	
1.1	*Introduction*	1
1.2	Statement of the problem	1
1.3	Approaches to problem-solving	2
1.4	Nanocomposites Materials	2
1.5	Nanocomposite Coating:	3
1.6	Thesis Outline	3
1-7	*Aim of This Work*	4
	Chapter Two Theoretical Part and Literature review	
2.1	Introduction	5
2.2	Theoretical Aspects	5
2.3	Corrosion Definition	5
2.4	Corrosion of Low Carbon Steel:	6
2.5	Corrosion Mechanism	6
2.6	Mechanisms of Carbon Steel Corrosion in Concentrated Sulfuric Acid	8
2.7	Types of Corrosion in Low Carbon Steel	10
2.7.1	Uniform corrosion	11
2.7.2	Galvanized corrosion	11
2.7.3	Crevice corrosion	12

2.7.4	Pitting corrosion	12
2.7.5	Erosion – Corrosion	12
2.8	*Corrosion Prevention and Control*	13
2.9	Corrosion costs:	14
2.10	Corrosion Prevention and the Role of Coatings:	15
2.11	Deposition Techniques	17
2.12	*Sol-Gel Processing*	18
2.12.1	Chemistry of sol-gel	19
2.13	Properties of Titanium Dioxide	21
2.14	Alumina:	22
2.15	Factors That Affect Sol-Gel Chemistry	23
2.16	Benefits and Drawbacks of Sol-Gel	24
2.17	Methods for Applying Sol-Gel	25
2.17.1	*Spin coating*	26
2.17.2	*Dip coating*	27
2.18	Design of Experiments (DOE)	28
2.19	Response Surface Optimization Method (RSM)	28
2.19.1	Minitab Software	29
2.20	*Literature Review*	30
	Chapter Three Experimental Part	
3.1.	Introduction	33
3.2.	Program of the Present Study	33
3.3.	Samples Preparation	35
3.4	Materials used in the preparation of coatings.	36
3.5	Preparation of the TiO_2- Al_2O_3 Nanocomposite coating	37
3.6	Preparation of the powder	42

3.7	Calcination	42
3.8	dip coating	43
3.9	Tests and inspections	44
3.9.1 1	inspection	44
3.9.1.1	*X-ray Diffraction (XRD)*	44
3.9.1.2	Scanning Electron Microscope (SEM)	45
3.9.1.3	Optical Microscope Analysis	45
3.9.2	mechanical tests	46
3.9.2.1	nanoindentation test	46
3.9.2.*2*	Pull-Off Adhesion Test	47
3.9.2.*3*	Measurements of coating thickness	48
3.9.2.*4*	Contact Angle Measurement	49
3.9.3	Corrosion Test	50
3.9.3.1	Electrochemical test (polarization test)	50
3.9.3.2	Erosion-corrosion test in concentrated Sulfuric acid	51
	Chapter Four Results and Discussion	
4.1.	*Introduction*	55
4.2.	*Results of Physical and Mechanical Tests*	55
4.2.1	*X-Ray Diffraction Analysis*	55
4.2.2.	*Optical Microscope Analysis*	57
4.2.3	Thickness test	60
4.2.4	*Pull-off testing*	63
4.2.5	Nano hardness test	65
4.2.6.	Potentiodynamic polarization	67
4.2.7.	Erosion- Corrosion test	71
4.2.8.	Contact angle	73

4.3.	Mathematical model	75
4.4	Optimization	77
4.5.	Confirmation of results for optimal sample	78
4.5.1	A. X-Ray Diffraction (XRD) Analysis	78
4.5.2	AFM TEST	79
4.5.3	SEM TEST	79
	Chapter Five Conclusions & Recommendations	
5.1	Introduction	81
5-2	Conclusions	81
5-3	Suggestions for Future works	81
References		85

List of Figures

No. of Figure	Description	No. of Page
	Chapter Two Theoretical Part and Literature Review	
2.1	Corrosion Mechanism	8
2.2	Erosion-Corrosion of steel pipe at high-velocity Sulphuric acid	9
2.3	Pitting corrosion in metals	12
2.4	Inside the mechanism of erosion-corrosion a pipe	13
2.5	Schematic showing classification of (surface modification and coating deposition) techniques	16
2.6	Schematic illustration of the routes that could be followed in sol-gel processing	19
2.7	Unit cell of Titanium dioxide	21
2.8	Representation of the crystal structures consisting of Anatase	21
2.9	Aluminum oxides' structure (alumina structure)	22
2.10	Fundamental stages of sol-gel TIO_2:AL_2O_3 preparation and deposition by dip and spin coating	25
2.11	Schematic of the spin-coating process	27
2.12	Stages of the dip coating process: dipping the substrate into the coating solution, wet layer formation by withdrawing the substrate, and gelation of the layer by solvent evaporation	28
	Chapter Three **Experimental Part**	
3.1	Flow chart of the experimental part of this work.	35
3.2	Materials used in the preparation of coatings	37
3.3	Flow chart of the stages of the synthase's sol of TiO_2, TIO_2-AL_2O_3	39
3.4	(a) sol,(b) gel	40
3.5	(A) stages of the synthases powder of tio2, tio2:al2o3, and(B) set of the preparation coating film	41
3.6	(A) before calcination,(B) after calcination	43
3.7	dip coating	43
3.8	X-ray diffraction machine	45
3.9	optical microscope	46
3.10	(A)diagram of the indenter (B) test-taking points	47
3.11	diagram of the dolly and substrate	48
3.12	The device of thickness measuring	49
3.13	Contact Angle	50

3.14	polarization test	51
3.15	Diagram showing the mechanism of the (Erosion -corrosion) Examination	52
	Chapter Four **Results & Discussion**	
4.1	XRD patterns of all sample	57
4.2	Optical micrographs of the surface	59
4.3	The effects of temperature, alumina content, and the number of layers on thickness	61
4.4	The effects of temperature, alumina content, and a number of layers on adhesion.	64
4.5	The effects of temperature, alumina content, and a number of layers on hardness.	66
4.6	Polarization curve of all sample	69
4.7	The effects of temperature, alumina content, and a number of layers on corrosion.	70
4.8	The effects of temperature, alumina content, and a number of layers on Erosion – Corrosion.	72
4.9	contact angle of all sample	74
4.10	Actual versus Predicted plot: (A) hardness level, (B) adhesion,(C) corrosion rate, (D) erosion-corrosion, and (E) thickness.	75
4.11	Actual versus Predicted plot: hardness level, adhesion corrosion rate, erosion-corrosion, and thickness.	77
4.12	XRD patterns of TiO2-based coating	79
4.13	three-dimensional AFM images of the TiO_2–10 wt.% Al_2O_3 nanocomposite film with 2 layers thicknesses.	80
4.14	SEM image of TiO2-AL2O3 surface morphology	80

List of Tables

No. of Table	**Description**	No. of page
	Chapter Two Theoretical Part and Literature Review	
2.1	shows the difference between the latest known coating methods.	17
	Chapter Three Experimental Part	
3.1	design of experiments in the Present Study	34
3.2	chemical composition of carbon steel (substrate)	36
3.3	Proportions of the constituent elements of metal rods	36
3.4	materials used in preparing the coating material	37
3.5	molar ratio of the materials used in preparing the coating material.	38
3.6	properties of H2SO4 in the pipe	53

	Chapter Four Results and Discussion	
4.1	Crystallization ratio and crystallite size analysis of XRD test	56
4.2	ANOVA Results for thickness	61
4.3	shows the results obtained for all tests	62
4.4	ANOVA Results for adhesion	65
4.5	ANOVA Results for hardness	67
4.6	ANOVA Results for corrosion rat	70
4.7	ANOVA Results for Erosion – Corrosion	72
4.8	Confirmation results.	78

List of Abbreviations

Abbreviations	**Meaning**	**unit**
ANOVA	Analysis of variance	
DF	Degree of freedom	
MS	Mean of squares	
SS	Sum of squares	
F	Fisher ratio	
P	Value of Probability	
Icorr	Corrosion current	Ampere
Ecorr	Corrosion voltage	Volt
Icorr	Corrosion current density	($\mu A/cm^2$)
XRD	X-Ray Diffraction	
SEM	Scanning electron Microscope	
ASTM	American Society for Testing and Materials	
Mpy	Mil per year	
A	Acid-exposed surface area	cm^2
W_0	Origin weight/	gram
W_1	Weight after immersion in Acid	gram
IP%	The improvement percent	
C.R.	Corrosion Rate	

Chapter

1

Introduction

1.1 Introduction

Steel, which has the broadest range of uses of any engineering material, is one of the most significant categories of materials. Depending on the amount of carbon in the steel, it may be classified as high, medium, or low carbon steel. Low carbon steel with a carbon content ranging from 0.15 to 0.35 wt% is used in various industrial processes and application fields [1,2]. Low carbon steel is used for structural applications in buildings, bridges, ships, and automobiles [3] because of its comprehensive manufacturing qualities, high ductility, and moderate strength. Low carbon steel stability and corrosion resistance in various environments are significant. But in a humid climate, steel is susceptible to rust and pollution, which may seriously limit its use. Metals and their surroundings interact electrochemically in a process known as corrosion. Because corrosion negatively impacts every aspect of human existence, companies must avoid it [4]. Therefore, it is desirable and necessary to have a low carbon steel surface coating resistant to corrosion and contamination [5]. The coating is the most widely used way of regulating, or avoiding corrosion due to the variety of coating procedures and materials available for many circumstances [6]. Physical vapor deposition, chemical vapor deposition, electrochemical deposition, plasma spraying, and the sol-gel process are a most common methods used to deposit coatings on metals [7].

1.2 Approaches to problem-solving

The method used to treat the corrosion issue in manufacturing included coating carbon steel with ceramic material (TiO_2-Al_2O_3). Using sol-gel to create coatings made of nanocomposites. The operating conditions of a pipe carrying concentrated sulfuric acid (98%) were considered a case to study in this search, and apply special tests for corrosion rate based on the technology of surface

modification as one of the solutions and treatments to protect against corrosion and reduce its rate. If successful, it is generalized to the rest of the factory parts.

1.3 Nanocomposites Materials

Along with the advancements in science and technology over the last 10 years, the field of nanophase materials and technology has emerged as a new application technology. Because nanocomposites have the potential to be used in a wide variety of applications, including biomedical, catalytic, separation, chemical sensing, fuel cells, capacitors, microfabrication, tribological, resonant coupling, and high flux gas transport [8], they have garnered a great deal of attention. Nanocomposite materials are complex combinations of nanophase materials and other components that enhance the effectiveness of traditional materials. These materials are also known as nanocomposites. Polymerization, sol-gel synthesis, deposition, sputtering, supercritical fluid synthesis, and laser synthesis are just some of the many methods used to synthesize various nanocomposites. Composites result in material properties that cannot be produced by either phase alone. In the past, composites were traditionally reinforced using inclusions on the micrometer scale. In recent years, processing methods have been developed that allow the size of inclusions to be reduced to the nanoscale [9].

1.4 Nanocomposite Coating:

The nanocomposite coatings comprise at least two incompatible phases and are separated by an interface region. It is required that at least one of the dimensions of the material be on the nanoscale. The primary constituent is the matrix, and fillers are distributed in this medium [10]. The fundamental aim of combining several materials into a single coating is to produce a brand-new nanocomposite material superior to both of the individual elements in terms of its

qualities and benefits. The nanocomposite coating increases the surface's mechanical qualities and corrosion resistance. In addition to this, they are capable of reducing the amount of corrosion that occurs in a variety of different ways. The formation of a passive layer on the surface of the nanocomposite coating offers a barrier resistant to corrosion. Furthermore, reducing the amount of oxygen present on the steel surface may result in low overpotential areas and decrease the number of corrosion processes on the surface.

1-5 Aim of This Work

The objective of this research is to reduce the rates of corrosion of equipment in the concentrated sulfuric acid factory (98%), one of the factories of the Al-Furat State Company for Chemical Industries and Pesticides/Ministry of Industry and Minerals.

1- Investigating the corrosion behavior by (Erosion – corrosion / Potentiodynamic polarization) for low carbon steel alloys coated by (TiO_2:Al_2O_3) nanocomposite in a high concentration of H_2SO_4 medium.

2- Study the physical and mechanical properties of prepared nanocomposites coating.

Chapter

2

Theory and Literature Review

Chapter Two

Theoretical Part and Literature Review

2.1 Introduction

This chapter provides an overview of corrosion, its many forms, and the various strategies that may be used to guard against it. It is a surface modification technique that protects surfaces from corrosion by addressing corrosion caused by erosion caused by concentrated sulfuric acid in carbon steel, metallic, and composite coatings. It deals with corrosion as a consequence of erosion. They also discuss the statistical approach utilized in the study and previous studies that employed techniques comparable to the method used in the research.

2.2 Theoretical Aspects

In this part, we will take a high-level look at the basic concepts of producing a coating layer utilizing the sol-gel technique. In addition, it explains what is meant by the phrase "sol-gel," as well as the most beneficial applications and negatives. In addition, it explains the kind of corrosion that occurred in the pipe containing H_2SO_4.

2.3 Corrosion Definition

Corrosion is the degradation or destruction of a substance due to interactions with its surroundings is what is meant when we talk about corrosion. Metals and non-metals are both included in this definition. According to temperature, low and high-temperature corrosion may be divided. Corrosion may alternatively be categorized as chemical or electrochemical. Corrosion may also be categorized as either wet or dry. Steel corrosion by an aqueous electrolyte is one form of wet corrosion [11].

2.4 Corrosion of Low Carbon Steel:

Corrosion is "the physical-chemical interaction between a metal and its environment, which leads to changes in the characteristic of the metal and which may often lead to impairment of the function of the metal [12]. The most significant factors contributing to corrosion development are the corroded component and the surrounding environment [13]. Corrosion is a natural process, and all-natural processes strive to reach the lowest feasible energy states as rapidly as possible. Corrosion is no exception to this rule. Steel and iron, as a result, have a natural inclination to interact with other elements and revert to their lowest energy levels. This is because they are both reactive elements. When combined with iron and steel, oxygen and water often combine to produce new compounds. These components, which contain the same chemical components as the initial iron ore, are present in the most natural electrolyte that has the potential to generate rust [14]. Rust may be formed when iron reacts with oxygen in the air. Several factors, including chloride, sulfate, humidity, and temperature, may make corrosion progression more complex in various ways, leading an increased risk of corrosion on low-carbon steel [15].

2.5 Corrosion Mechanism

The electrochemical response is inextricably linked to the corrosion process and cannot exist without it. Electrochemical methods need the transfer of electrons between different atoms. A redox reaction will always result in the displacement of electrons (oxidation-reduction). An anodic reaction is part of the process that allows corrosion to occur due to electrochemical reactions. Indicators of anodic processes, also known as oxidation, include valence or electron product rise. The

following equation describes the anodic reaction that takes place when metal is corroded [16]:

$M \rightarrow Mn^{+} + ne$ ………………………………………. (1)

During corrosion of metals, the metal is oxidized to produce one ion (n+) in the electron n emission process. As an example, iron's n is influenced by the metal's properties:

$Fe \rightarrow Fe^{+2} + 2e$ ………………………………………(2)

The cathodic reaction is used as part of the corrosion process as well. The drop in valence value that occurs as a consequence of the anodic reaction is an indication of the cathodic response. Another indicator is the consumption of electrons. The reaction occurs when oxygen from the air dissolves in an open solution during a cathodic reaction. The following is a written explanation of the corrosion process that takes place in iron (Fe):

$Fe\ (s) + H_2O\ (l) + \frac{1}{2}\ O_2\ (g) \longrightarrow Fe(OH)_2\ (s)$…… .....…………(3)

Ferric hydroxide [$Fe(OH)_3$], a transient (temporary) result, may be produced spontaneously when Ferro hydroxide [$Fe(OH)_2$] is oxidized by water and oxygen. This reaction process is as follows:

$4\ Fe(OH)_2\ (s) + O_2\ (g) + 2\ H_2O\ (l) \longrightarrow 4\ Fe(OH)_3\ (s)$ ………..(4)

Rust is the term used to describe the brownish-brown Fe_2O_3 that results from the hydroxide ferries. Vogel (1979) noted the following reactions:

$2\ Fe(OH)_3 \rightarrow Fe_2O_3 + 3\ H_2O$ …………………………..(5)

In most cases, the oxidized metal is the starting point for corrosion in a solution. This metal then gives off electrons, which results in the generation of positively

charged metal ions. As a consequence of the reduction in the amount of H^+ and H_2O ions, the solution will function as a cathode, releasing H_2 and lowering the amount of O_2. As a consequence of the metal being repeatedly dissolved in the solution, the surface of the metal undergoes reactions that cause exfoliation. These reactions take place on the surface of the metal. The mechanism of corrosion on the surface of the metal is shown in figure (2.1) [17].

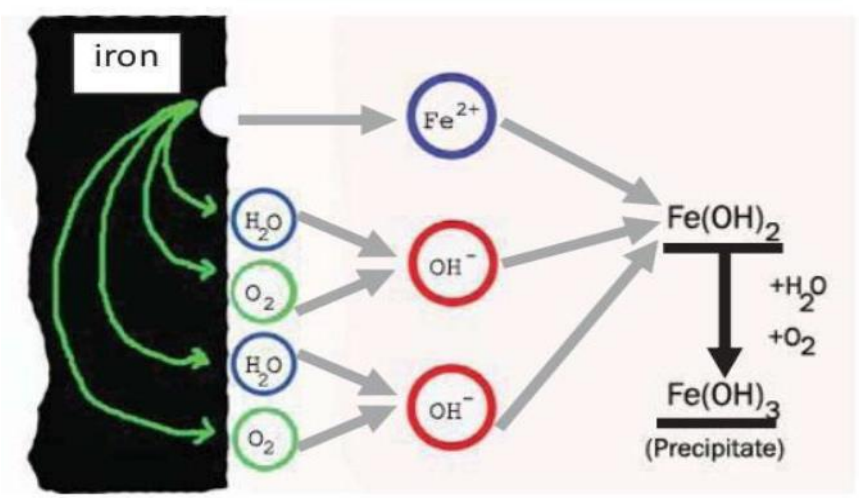

Figure 2.1 Corrosion Mechanism [18]

2.6 Mechanisms of carbon steel corrosion in concentrated sulfuric acid

In the concentrated sulfuric acid factory, the carbon steel tubes that carry concentrated sulfuric acid (H_2SO_4) are corroded because they are exposed to sulfuric acid. However, depending on the kinetic state of the acid, the impact of corrosion on carbon steel will be increased to a greater degree. When we talk about the "kinetic state of the acid," what we really mean is the condition of stagnation that takes place when acid is kept in tanks. The second possibility includes the condition of the acid, that is known as the flow state, which takes place when acid is moved through tubes. When carbon steel is exposed to concentrated sulfuric

acid, a chemical reaction takes place that results in the formation of ferrous sulfate, which is denoted by the formula $FeSO_4$ in reaction (6).

$$H_2SO_4 + Fe \longrightarrow FeSO_4 + H_2 \text{……..(6)}$$

The $FeSO_4$ will adhere to the surface of the steel, and over time it will form a barrier there. The metal under this layer is shielded from further corrosion that may be induced by concentrated sulfuric acid by this layer. Therefore, the preservation of the $FeSO_4$ layer is necessary to guarantee the carbon steel storage tanks' ability to withstand the test of time [19]. It is known as the effect of (erosion-corrosion) due to the flow of concentrated sulfuric acid, and it is illustrated in figure (2.2) [20]. If the acid flows at a speed that is faster than the critical speed, the protective layer ($FeSO_4$) will be damaged as a result of the acid flowing quickly, and the steel surface will be exposed and corrode.

Figure (2.2): Erosion-Corrosion of steel pipe at high-velocity Sulphuric acid [20]

2.7 Types of Corrosion in Low Carbon Steel

There are several different categories that corrosion may be placed into. Dry, wet, and molten-matter corrosion are the three primary types of corrosion that can occur on metallic materials. These types of corrosion are classified according to the media that cause the corrosion: fluids and molten metals are included in the molten-matter corrosion category. Wet electrochemical reactions are those in which water-based electrolyte, and the corrosive environment is created by using water. A corrosive environment is said to be dry corrosion, which may happen when a dry gas is present [21]. Because it has both physical and mechanical qualities, low carbon steel is often used as a structural material in a wide variety of industrial applications. However, it is susceptible to corrosion in marine and industrial conditions, particularly in acidic solutions, which are often found in industrial environments [22,23]. This vulnerability is especially pronounced in acidic solutions. The oxidation of the metal that occurs during the anodic reaction may be represented by the following equation: [24]

$$Fe \rightarrow Fe^{+2} + 2e^{-} \quad \text{..... (7)}$$

Oxygen, which is very soluble in water, is a possible acceptor of electrons. According to the reaction, there is oxygen depletion in neutral or alkaline solutions.

$$O_2 + 2H_2O + 4e^{-} \rightarrow 4OH^{-} \quad \text{..... (8)}$$

2.7.1 Uniform corrosion

It is described as the gradually decreasing metal thickness resulting in a reasonably uniform effect throughout the surface. The lifetime of the equipment may be realistically anticipated since the degradation is linear over time, making it

the most common damage. It is uniform because it is created by several anodic and cathodic zones that form, disintegrate and move over the surface over time. While contact with the environment is often the salt water, soils, and chemicals may exacerbate the problem [25]. It is universally recognized as the most widespread of all forms of corrosion. Still, the minor damage in terms of failure number, corrosion that is uniform spreads when there are no sites that are preferential on the surface that is more preferred for attack than the other one; hence, all areas are uniform, and equivalent dissolution occurs. Two features of uniform corrosion need to be considered carefully: the corrosion rate and susceptibility. The corrosion rate determines how much a material will be corrupted in a given time interval calculated in the equation. In contrast, exposure to corrosion is the material's tendency to corrode. It is the thermodynamic function, especially the potential energy required to oxidize and decrease species present in the corrosion cell. The most quoted instance used to prove corrosion is the formation of rust, the powder that is orange-red colored, which is commonly available at the iron surface, in the complex that is hydrated Fe_2O_3.The anodic oxidation of iron and the cathodic reduction of oxygen produce H_2O [26].

2.7.2 Galvanized corrosion

When two various metallic materials are linked electrically and put in a conductive solution, a potential that is electrical will be available. This difference of potential will give a driving force that is stronger for the less noble (which is more negative electrically) material dissolution. It will also decrease the inclination for the material, which is nobler to dissolve [27].

2.7.3 Crevice corrosion

Corrosion deposits form in areas of metal that are not immediately exposed to the environment, such as flanged joints and lap joints because the protective coating covering the metal has been altered or destroyed in some way [28].

2.7.4 Pitting corrosion

It is referred to as an attack that is localized and corrosive of a passive metal that results in the development of small cavities (pits). Their growth leads to the perforation of a pipe wall or metal plate [29]. Figure (2.3) Shows a diagram of Pitting corrosion.

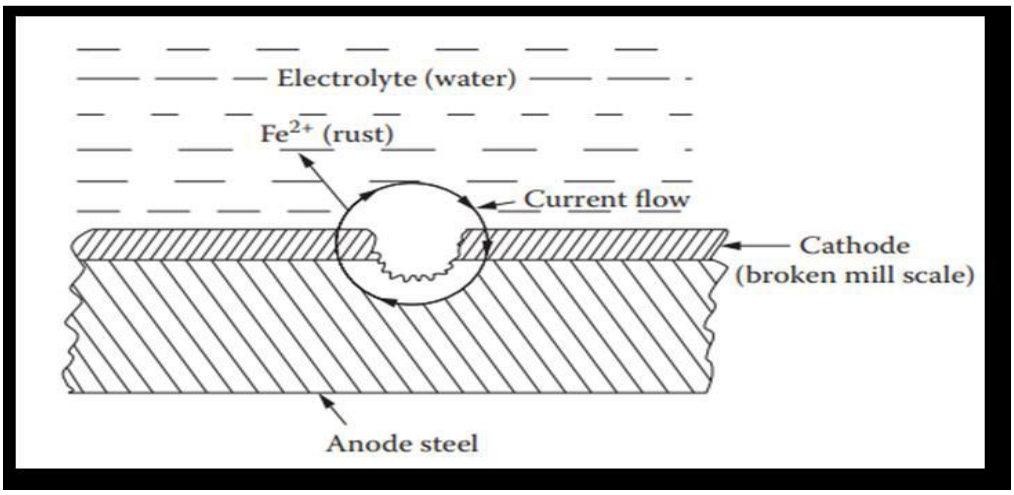

Figure (2.3): Pitting corrosion in metals [30]

2.7.5 Erosion – Corrosion

The process of material deterioration brought on by mechanical action may be depicted with the assistance of solid particles, liquid, or a mixture of both processes. The size, shape, and velocity of these particles all have a significant impact on the pace at which wear occurs. This process happens when a mechanical action or corrosion by solid particles combines with a chemical assault resulting

from the dissolution or oxidation of surfaces on metallic objects, which removes or scratches the surface layer. This may also be referred to as erosion-corrosion. Corrosion is a term that may be used to describe the process of material deterioration. The combination of erosion-corrosion results in more excellent rates of metal than the addition of the individual wear rates caused by pure erosion and flow corrosion. The concept of complementarity inspired the creation of the term "synergy." By eliminating the passive protective coating and exposing the underlying metal surface to the corrosive media, oxidation may exacerbate corrosion in hot, acidic situations [31,32]. Figure (2.4) shows a Pipe deterioration and corrosion mechanisms seen from the inside.

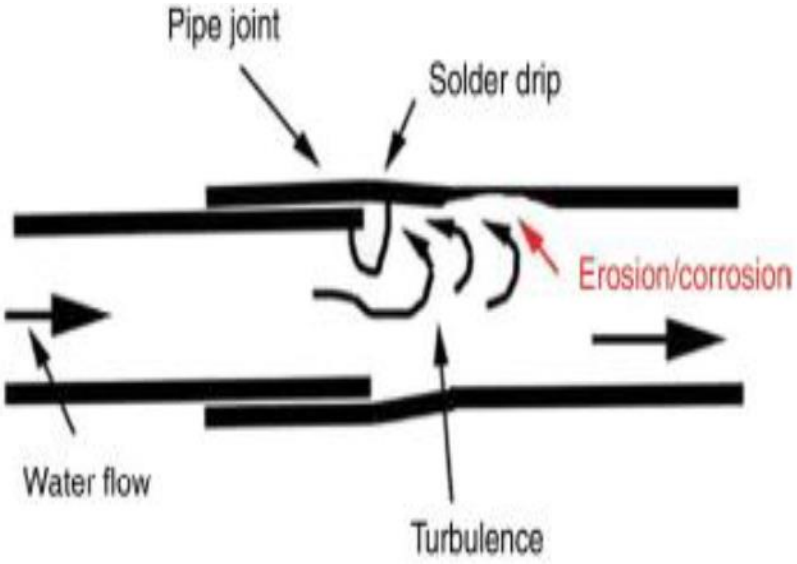

Figure (2.4): Inside mechanism of erosion-corrosion a pipe [33]

2.8 Corrosion Prevention and Control

Since metal corrosion occurs due to aggressive species that have already reacted with metal and are present in the electrolyte, a prominent method for protecting superior corrosion would be to prevent these species from reaching the

metal surface. This may be accomplished using a variety of approaches,]including the following[34:

1- Choose the material that is the most appropriate.

2- Determine which design is most appropriate for the component or the system.

3- Changes made to the surrounding environment

4- Changes that can be made to the potential.

5- The use of either an anodic or a cathodic protection method.

6- The use of compounds that impede.

7- Use coatings that are protective.

8- Make sure there is sufficient ventilation and drainage to cut down on the amount of condensation that builds up.

9- Staying away from low-lying locations that have poor drainage [35]

2.9 Corrosion costs:

In three ways, corrosion adds to the cost of living in society: it is very costly, wastes natural resources when environmental degradation is a growing issue, and sometimes puts people's lives at risk. There are still many adverse effects of using corrosion for good, including chemical machining, anodizing, graving, etc. Aesthetic deterioration, high operating and maintenance costs, plant shutdowns, product pollution, missing essential components, protection and durability impacts, and the new product liability pattern where providers are accountable instead of customers are some of the adverse effects [36]. The cost of corrosion is considerable and affects numerous industries, residential uses, and the public

sector globally, highlighting the need for adequate corrosion controls. The cost of corrosion alone is projected to be (USD) (170) billion a year, making it one of the most challenging tasks in the oil, gas, and chemical industries. Losses include the high price of corrosion and the environmental and health risks linked to the potential loss of oil and gas equipment, which drive the global development of corrosion-resistant materials and cutting-edge corrosion avoidance techniques [37].

The installation, operation, and repair of anti-corrosion technologies may be used to determine the economic cost of corrosion directly. In contrast, indirect production losses, loss reimbursement, environmental damage, etc., can be used to determine the corrosion cost indirectly. [38]. The following definition should apply to the cost of corrosion:

1- Costs of prevention: the price of each action deployed, maintained, or improved to assure corrosion avoidance.

2- Costs associated with examining, assessing, and monitoring the corrosion management plan.

3-. Maintenance costs: the money spent to keep equipment in good functioning order. For behavior that meets the criteria specified.

4- Administrative costs: the price of each managerial choice to look into, lessen, or pass the danger of corrosion [39].

2.10 Corrosion Prevention and the Role of Coatings:

The process of adding a thin layer termed a coating to the surface of base metal, sometimes referred to as the substrate, is called coating. The primary objective of the coating is to increase the material's resistance to corrosion. Coatings may be applied at a wide range of temperatures to either the interior or

the outside of a surface, producing smoother surfaces and increasing the coatings' efficiency. [40].

By changing the surface of metallic substrates with nanocrystalline coatings, nanomaterials are thought to potentially reduce the rate of corrosion. It is generally accepted that anything with a size of 100 nanometers (100 millionths of a millimeter or 100 billionths of a meter) or less is considered to be within the realm of nanotechnology. Nanotechnology is the umbrella term for the process of designing and fabricating anything whose function is dependent on a specific structure at the nanoscale. It encompasses things like machines or systems manufactured by adjusting the positions of individual atoms or molecules and substances with microscopic features. Figure (2.5) shows a diagram of the essential coating and surface modification processes.

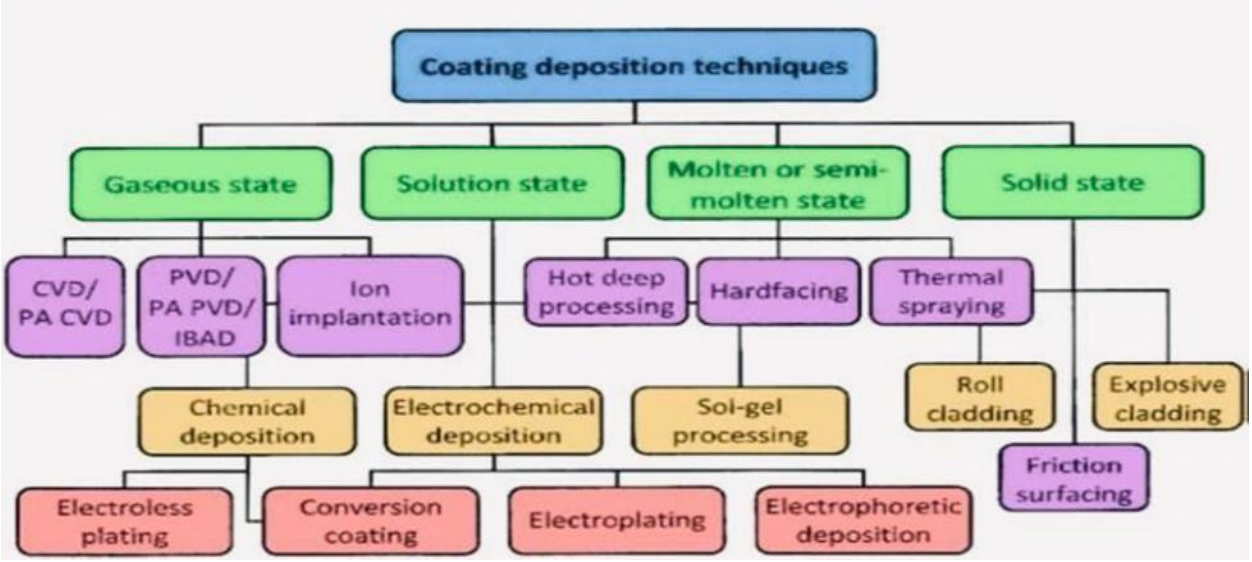

Figure (2.5): Schematic showing classification of (surface modification and coating deposition) techniques [41].

The qualities of the material employed may sometimes be improved using nanomaterials since they have a wide variety of valuable features, including thermal, mechanical, physical, chemical, and optical capabilities [42]. This is because their small size permits the production of larger attraction forces between nanoparticles [43]. Nanoparticles significantly influence coatings among the many corrosion protection techniques.

2.11 Deposition Techniques

There are many techniques capable of depositing a nano-layer of ceramic on metals. The processes of So-Gel coating, plasma spraying, and electrochemical deposition are the ones that are used the most commonly.

Table 1 summarizes the benefits and drawbacks of each approach.

Approach	Thickness	Benefits	Weaknesses	References
Sol-gel	<1 μm	Low temperature required for processing, low cost, and produces a coating that is both pure and extremely thin, on both flat surfaces and intricate forms.	Poor adhesion to the substrate and a controlled atmosphere is required in some stages.	[[44]–[45]]
Plasma spraying	<20 μm	A process with a lower possibility of coating deterioration, quick deposition, and a high cost.	Non-uniform coating density, poor adhesion, and high processing temperature	[46]
Electrophoretic deposition	100–2000 μm	Complex forms, homogeneous thickness, and fast deposition.	High processing temperature and difficulty in producing a crack-free coating	[47]

2.12 Sol-Gel Processing

Manufacturing ceramic materials created from brine is referred to as "sol-gel," a famous phrase for the process. Ceramic particles are distributed throughout the sol. A liquid in which colloidal particles are suspended is another definition of what is known as a colloidal solution. A semi-solid mass is generated when colloidal particles are bonded to create a network or when ceramic particles are interconnected to form a gel. This mass may also be referred to as a gel. [48].

Over the past few decades, there has been an increase in interest in the sol-gel process because it makes it possible to develop new materials and new shaping routes (fibers, thin films, and near net shape objects) with good homogeneity and good purity. This has contributed to the increase in interest. In addition, it is anticipated that the sol-gel technique will be particularly effective for producing ceramic materials, which must be sintered into a solid body [49]. The sol-gel approach produces tiny nanoparticles with high chemical reactivity and superior purity, homogeneity, and physical qualities to those produced by traditional high-temperature procedures. In addition, the sol-gel method produces more nanoparticles per unit of time. This technology offers a cost-effective and easy way to create mono- and multicomponent glasses and ceramics, which would not be accessible if they were prepared using traditional procedures [50].

The many paths that may be taken in the sol-gel processing are shown in a schematic form in figure (2.6). The structure of the gel, in addition to the chemical consistency of the gel as a whole, is significantly impacted by the chemical processes that take place during the transformation of the precursor solution into the gel. Understanding how the speeds of chemical reactions are governed by the processing factors such as the chemical composition of the precursor,

concentration of reactants, pH of the solution, and temperature [48] is thus a fundamental challenge.

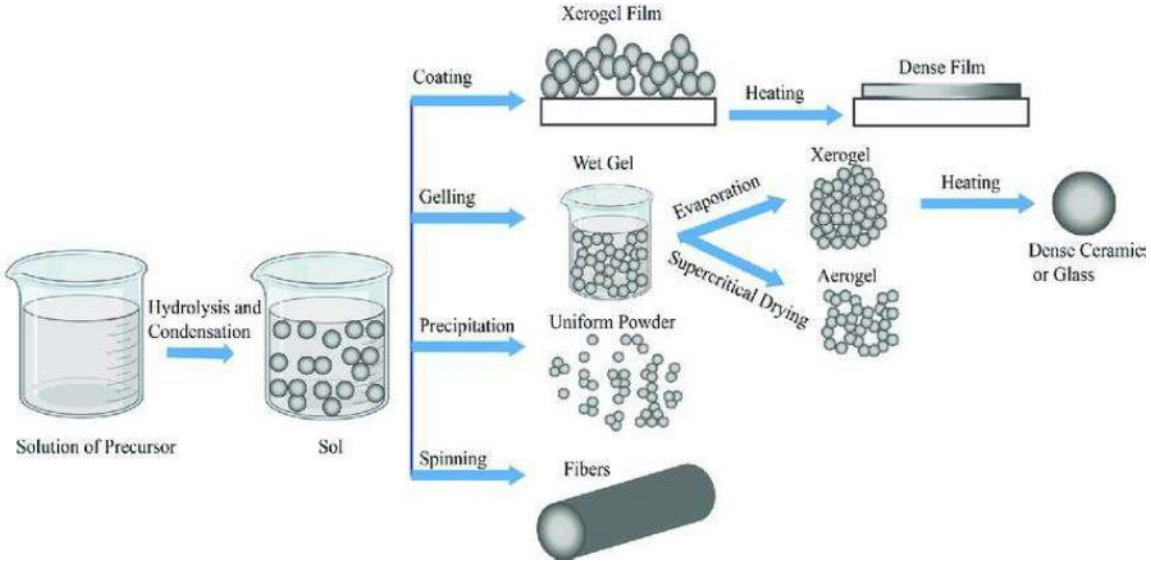

Figure (2.6): Schematic illustration of the routes that could be followed in sol-gel processing [48].

2.12.1 Chemistry of sol-gel

The sol-gel method is an inorganic polymerization process resulting from water or another solution that converts a solution of an organic substance into an inorganic solid. An organometallic compound, such as an alkoxide, or an inorganic mineral salt, is often used as a starting or starting material (chloride, nitrate, sulfate, etc.). Metal alkoxides are the most widely used raw materials because they react effectively with water and are famous for many minerals.[51]. The stages that make up the sol-gel procedure are as follows:

1. Creating a homogeneous solution may be done by dissolving inorganic salts in water or metal-organic precursors in an organic solvent that is miscible with water. Both of these methods result in the same solution.

2. To turn the homogeneous solution into a sol, apply the suitable reagent to it.

3. Aging.

4. Sintering and other forms of heat treatment. The first step of the sol-gel process involves converting the precursor material into a highly bonded solid. This stage follows the previous one, which includes the operations of hydrolysis and condensation, which eventually culminates in the manufacture of high purity ceramic powder. The gel is a connected, solid, and porous inorganic network that encases a continuous liquid phase. Gels can be made from a variety of materials. A colloidal solution is produced as by product of hydrolysis, defined as the dispersion of colloidal particles in a liquid. [52].

Hydrolysis and condensation are the two primary reaction types involved in the sol-gel conversion of metal alkoxides. As a result of the oxygen atom in a water molecule being attacked nucleophilic ally during hydrolysis, the alkoxide groups (-OR) are exchanged, releasing alcohol and creating metal hydroxide. Oxidation reactions involving two hydroxylated metal species produce M-O-M bonds under the release of water. In contrast, M-O-M bonds under the release of alcohol are produced by reactions between hydroxide and an alkoxide (alkoxolation).

$$M\text{-}OR + H_2O \longrightarrow M\text{-}OH + ROH \text{ (Hydrolysis)} \quad \ldots\ldots\ldots\ldots (10)$$

$$M\text{-}OH + HO\text{-}M \longrightarrow M\text{-}O\text{-}M + H_2O \text{ (condensation)} \quad \ldots\ldots\ldots (11)$$

$$M\text{-}OR + HO\text{-}M \longrightarrow M\text{-}O\text{-}M + ROH \text{ (alkoxolation)} \quad \ldots\ldots\ldots (12)$$

Where; M: the metal atom (Si, Zr, Ti, Zn, etc.…)

R: is the alkoxide group, and O: is the oxygen atom [53].

2.13 Properties of Titanium Dioxide

Titanium dioxide (TiO_2) is a naturally occurring mineral; three commonly known forms of TiO_2 design occur brookite, anatase, and rutile [54]. The Crystal Structure of Titania (TiO_2): As illustrated in fig. (2.7), oxygen surrounds titanium in an octahedral pattern; commercially, the anatase is tetragonal [54].

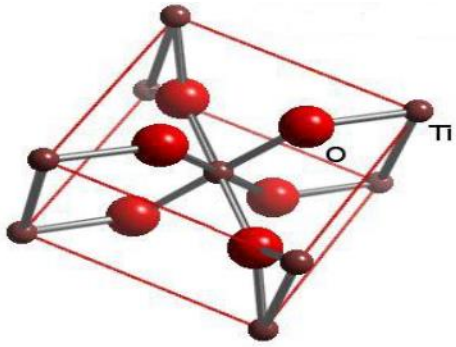

Figure (2.7): Unit cell of Titanium dioxide [55].

Anatase is a tetragonal mineral of octahedral habit. Figure (2.8) depicts the unit cell of anatase. The anatase type is more widely used in engineering applications because it has higher photocatalytic abilities than the other types of TiO_2. It is possible to represent the unit cell structures of anatase TiO_2 as chains of TiO_6 octahedra. In these structures, each Ti^{+4}ion is surrounded by an octahedron of six O_2 - ions (fig. 2.8).

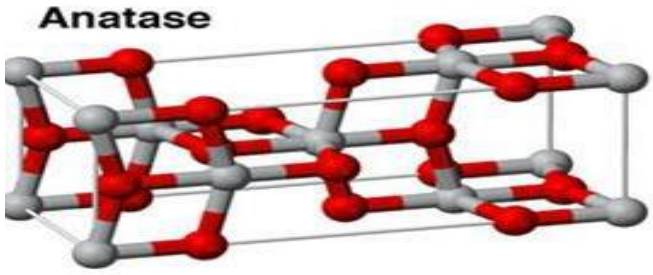

Figure (2-8): Representation of the crystal structures consisting of anatase [56].

2.14 Alumina:

Alumina is known to have good corrosion resistance and hardness. Al_2O_3 excellent resistance to abrasion and friction behavior is related to its surface smoothness and surface energy, and it adheres well to metal substrates when deposited as a coating on them. Al_2O_3 has been used in steel surface modification, heat transfer fluids employment, wastewater treatment, gas diffusion barriers, surface passivation, anti-reflection coatings, and other applications due to their outstanding mechanical properties and corrosion resistance. In addition, it has found widespread use in several technical disciplines, including abrasives, coatings, cutting tools, insulators, and composites. [56]. Alumina is used in applications requiring very high temperatures. It is an inert material that is hard, highly resistant to acids and bases, wear resistant, and insoluble in all common chemical reagents. Due to these characteristics, it is a smart material for various applications, from aerospace to health and medicine [57]. The structure of (Al_2O_3) is seen in Figure (2.9).

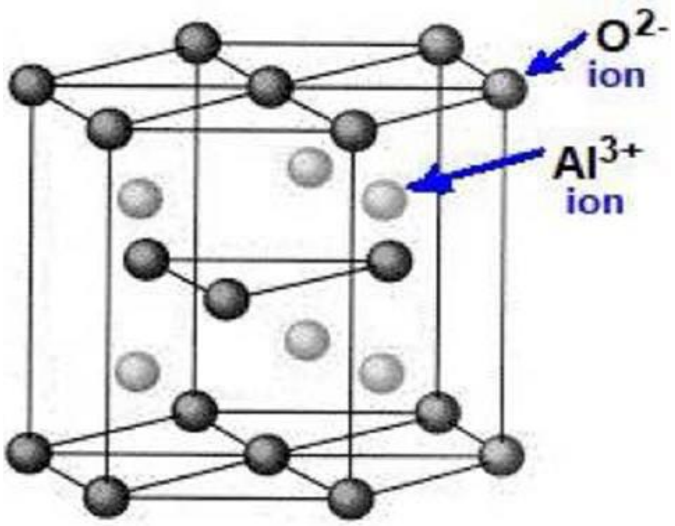

Figure (2.9): Aluminum oxides' structure (alumina structure) [58].

2.15 Factors That Affect Sol-Gel Chemistry

The following variables are often of significant importance to sol-gel chemistry:

1. PH: Any water-based colloidal chemistry is sensitive to pH [59].

2. Solvent: The solvent must maintain the nanoparticles dissolved while they group together (polymerize) into nanoparticles to prevent precipitation of the particles out of the liquid. Additionally, the solvent could aid in the bonding of nanoparticles. Because of this, the solvent significantly affects whether a gel network can develop [60].

3. Temperature: - Temperature has an effect on the longevity of the gel because it speeds up the chemical kinetics of the various processes that are involved in manufacturing nanoparticles and assembling nanoparticles into a gel network. If the temperature is too low, the gelation process might take many weeks or even months to complete. The actions that connect nanoparticles together to generate the gel network happen too quickly at a temperature that is too high, which results in the formation of clumps, and solid precipitates out of the liquid. [59].

4. Heat produced by reactions: Chemical reactions that result in the creation of nanoparticles and gel networks may emit heat that can flow back into the solution and speed up reactions while also releasing additional heat [61].

5. Time: Different processes in the gel formation process operate differently across various time periods, depending on the kind of gel being created. For sol-gel, slower is often preferable. A gel typically has a much more homogeneous structure when it is given time to slowly develop. Overly accelerated reactions lead to the formation of precipitates rather than gel networks, which may render gels weak and hazy or prevent them from forming all together [62].

6- Catalysts include Chemicals that speed up chemical reactions but are not themselves part of the process known as catalysts. Both acids (H^+) and bases (OH) operate as catalysts in many types of sol-gel chemistry, speeding up chemical processes in various ways. This is another factor contributing to the pH sensitivity of sol-gel chemistry. The gel time may often be drastically altered, going from hours, days, or weeks to minutes, by adding small quantities of catalysts (catalytic amounts) in the range of milligrams per tens of milliliters of solution [61].

2.16 Advantages and Disadvantages of Sol-Gel

A- Advantages of Sol-Gel :

1- The temperatures that must be reached for all processes other than sintering are quite low, and they are typically just a few degrees above room temperature [63].

2- Because there are no processes for grinding and pressing, relatively high chemical purity may be maintained [64].

3- The high surface area of the gels or powders generated by this method ultimately results in a sintering temperature that is lower than average[64].

4- As a result of the utilization of liquid precursors, it is possible to cast ceramic materials into a wide variety of intricate shapes, in addition to the production of thin film, fibers, powders, coatings, spheres, and monoliths, all of which can be accomplished without the utilization of machining or melting [63].

5- The low temperature required for the sol-gel processing method is often lower than the temperature at which oxide materials crystallize, which enables the creation of unique amorphous materials [65].

2- Sol-Gel Disadvantages[66]

a-Possible matrix breaking due to significant shrinkage.

b- Health hazards of organic solutions.

c- Low mechanical properties

d- Long processing times, particularly where careful aging and drying are required.

2.17 Methods for Applying Sol-Gel [66]

There are two different ways that Sol-Gel may be applied:

• The spin coating method, in which the optical surface spins while the Sol-Gel is put on top.

• A coating is applied by dipping, in which the substrate is submerged in the liquid.

The most popular coating methods that use the Sol-Gel technology are shown in Figure (2.10).

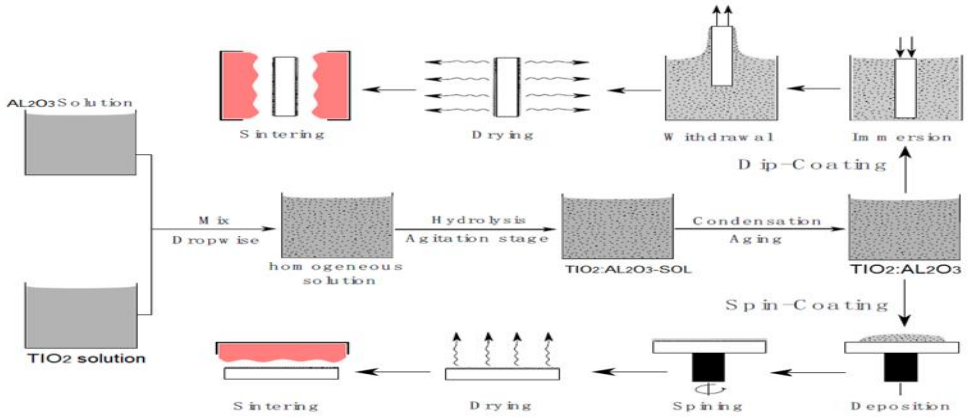

Figure (2.10)**:** Fundamental stages of sol-gel TIO_2:AL_2O_3 preparation and deposition by dip and spin coating [66].

2.17.1 Spin coating

The application of the spin coating is a technique that is used to deposit thin films that are homogenous across flat surfaces. In most cases, a minuscule quantity of coating material is applied to the center of the substrate, which is either spinning at a slow speed or is not spinning at all. After that, the substrate is spun at a high speed in order to make use of the centrifugal force in order to distribute the coating material. A spin coater sometimes referred to simply as a spinner, is a kind of machine that is used for spin coating.

The substrate is rotated continuously as the liquid is spun off the edges of the surface. This process is repeated until the film reaches the appropriate thickness. In most cases, the solvent administered is volatile and will concurrently evaporate. Therefore, the film will be thinner if the angular speed of the spinning is increased. Additionally, depending on the viscosity and concentration of the solution and the solvent, the thickness of the film might vary [67].

Spin coating, which may be utilized to produce homogeneous thin films with nanoscale thicknesses, is often employed in the microfabrication of oxide layers utilizing sol-gel precursors. In photolithography, it is often used to deposit layers of photoresist that are roughly 1 micrometer thick. Typically, the photoresist is spun for 30 to 60 seconds at a speed of 20 to 80 revolutions per second [68].

Due to the influence of centrifugal force, liquid flows radially, and any surplus is expelled off the substrate edge. The film keeps thinning gradually until either disjoining pressure forces it to attain an equilibrium thickness or until it solidifies as a result of a sharp increase in viscosity brought on by solvent evaporation. As shown in fig. (2.11) [69], solvent evaporation is the only factor responsible for the film's ultimate thinned state.

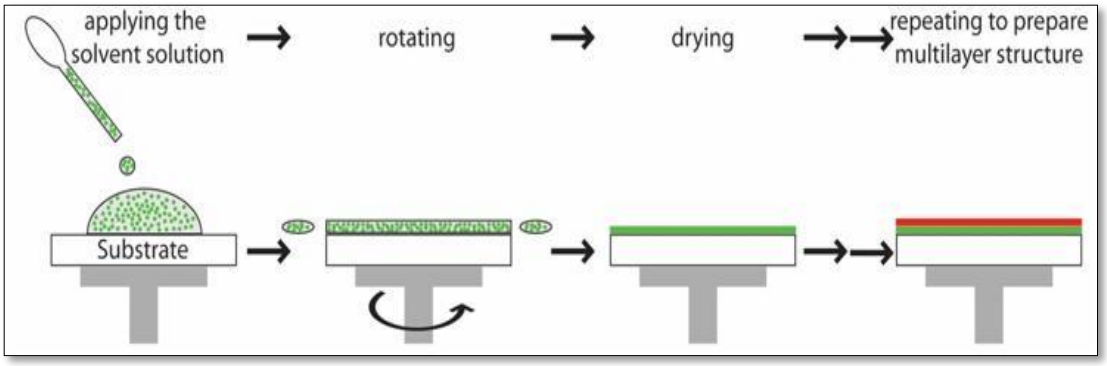

Figure (2.11) : Schematic of the spin-coating process [69].

2.17.2 Dip coating

Since dip-coating is a low-cost, waste-free technique that is simple to scale up and provides excellent control over thickness, it is the perfect approach for creating thin layers from chemical solutions [70]. Figure (2.12) [71] depicts the dip coating process' stages.

The benefits of this approach include [72]**:**

1- Thorough coverage

2- Rapidity.

3- Appropriate for objects that cannot be sprayed.

4- Dip coatings are profitable and safe for workers.

The drawbacks of dip coating , according to [72]**:**

1-There is a need for large quantities of coating and enormous tanks.

2- Because the paint moves slowly, gelling might happen.

3-The oil and grime from the items may contaminate the coat.

4- The item should not include any cavities to prevent the retention of liquid paint.

• A heater may sometimes be required to maintain a steady temperature.

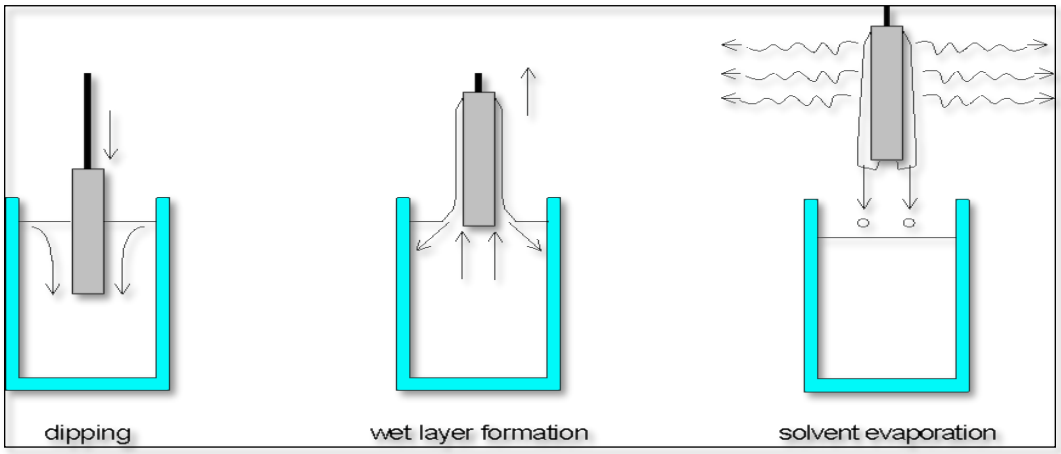

Figure (2.12): Stages of the dip coating process: dipping the substrate into the coating solution, wet layer formation by withdrawing the substrate, and gelation of the layer by solvent evaporation [72].

2.18 Design of Experiments (DOE)

It details the procedures for planning, evaluating, and arranging experiments so that it is possible to arrive at objective and valid findings in an efficient and adequate manner. To acquire statistical conclusions from an experiment, it is required to include both complex and simple statistical approaches into the strategy used to design the experiment. For every industrially organized experiment to be carried out effectively, there must first be careful planning, followed by selecting an appropriate design and then examining the collected statistical data.[73]. The response surface approach is a useful tool for optimizing the design of high-quality systems

2.19 Response Surface Method (RSM)

Response Surface Method (RSM) is an acronym that stands for Response Surface Method, and it refers to a group of statistical and mathematical approaches that may be used to design, improve, and optimize processes. [74]. The researcher

mainly concentrated on building and optimizing the empirical models in this work. To demonstrate that despite the use of a limited number of design variations, the proposed RSM methodology would yield sets of "best" design parameters that would cluster in a region of the design space response ,surfaces were computed using all 14 designs. Discovering the optimal response is the first and most important objective of the Response Surface Method. When there is more than one answer, it is vital to discover the compromise optimum, which does not maximize any one response. The second objective is to get an understanding of how the response varies in a certain direction as a result of changes made to the design factors. [75]. Experimentation is the backbone of the response-surface technique, which consists of a collection of different approaches to determining the optimal working circumstances. Typically, this entails carrying out several separate experiments, with the findings of each experiment serving as a point of departure for the subsequent steps. In this study, an RSM has been constructed via the use of the Minitab 17 programming language to run and estimate the response effects, as well as depict this impact by the suggested prediction model.

2.20 Literature Review

This literature review includes the previously published works that deal with sol-gel as general studies, with a particular focus on TiO_2-Al_2O_3 nanocomposite coating research.

Erdal Celik, and Ibrahim Keskin (2007) In this investigation, the sol-gel method was used to deposit a thin layer of TiO_2 - Al_2O_3 onto a glass basis. The formed phases, microstructure, hardness, adhesion measurements, and optical properties were studied. Four solutions containing different percentages of Al_2O_3-TiO_2 (0,0.075, 0.18, and 0.73) were generated, and aluminum chloride ($AlCl_3$ $6H_2O$) powder and titanium isopropoxide were used as sources of Al, Ti alternately. The results showed that the alumina improved the surface morphology, and the increased ratio of Ti led to increased adhesion. The microstructure of the surface layer showed the appearance of a mosaic shape of the surface layer. In addition, the acidity in the solution increases with an increase in the ratio of Al / Ti. This is due to the chlorine ions present in the source used for alumina, which causes an increase in the acidity of the solution[79] .

H. Vaghari and Z. Sadeghian(2011) Demonstrated the effect of TiO_2:Al_2O_3 nanocomposite coatings on stainless steel type 316L in 0.5 NaCl solution. Sol-gel technology was used in the production of the coatings, and the following experiments were carried out to validate the findings of the research (XRD, SEM, AFM FTIR, AFM). In addition, corrosion tests were carried out. Tetra-n-butyl titanate (TBT) was used as a source of Ti, aluminum isopropoxide ($Al(C_3H_7O)_3$) as a source of alumina, and 9 layers were coated on the base metal. The results showed that adding alumina greatly enhances the corrosion resistance, and the increase in the number of layers leads to surface roughness and a decrease in corrosion resistance [77].

P. Doodman and M. A. Faghihi-Sani (2013**)** In this study, . was used Both the sol-gel technology and the technique of coatings by dipping to create a nanostructured thin layer of coatings. The method of coatings by dipping is the more common of the two. X-ray diffraction and scanning electron microscopy (SEM), along with atomic force microscopy (AFM) for studying the topography of the surface and thickness, were utilized in this research project to investigate the influence calcination temperature and withdrawal speed had on the characteristics of the structure. Aluminum hydroxide sol was used as a source of aluminum. The XRD results showed that the alumina is still in a state of amorphous even at a temperature of 800, and the results also showed that the increase in the withdrawal speed leads to an increase in the thickness of the coatings layer. The results also showed that the alumina coatings have a high corrosion resistance [78].

Seyyed Alireza Oliaee and Sanaz Naghibi (2017) In this experiment, coatings made of nanostructured ceramic materials safeguard the surface of the steel. This study was directed to examine the protective effects of coatings containing Al_2O_3 and TiO_2 to obtain coatings without surface defects. XRD, FESEM, AFM, TAFEL, and ELS techniques were used, as well as accurate hardness measurement. Where the weight ratio of TiO_2:Al_2O_3 was 75:25 and at different temperatures, where the results showed that the alumina is still in a random state at a temperature of 800 and that the presence of alumina with Ti with enhances the anatase phase up to a temperature of 800 and that the heat treatment until a temperature of 900 led to the appearance of Al_2O_3 in addition to that, the corrosion resistance improved by 97% [76].

A. R. Simbar and A. Shanaghi (2020) This study directs attention to the protection of AA 2024-T3 alloy by a layer of coatings consisting of TiO_2 - Al_2O_3 - Benzotriazole by sol-gel technology and dip coatings. Aluminum tri-sec-butylate and tetra-n-butyl orthotitanate were used as a source of alumina and Titania,

respectively. The three solutions were prepared separately with different molar ratios for each material used. The three solutions were combined to form the coating material as a nanocomposite. The coating was done in several layers, corrosion tests were carried out, including immersion for 1:48 and 90 hours, and the corrosion rate was calculated. The results showed that the coatings with nanocomposites offer the best corrosion resistance because they give the lowest corrosion rate [80].

Chapter

3

Experimental Work

Chapter Three
Experimental Part

3.1. Introduction

This chapter provides clear picture of the experimental work that was done and details every one of the circumstances under which the tests were conducted. It comprises not only the physical and mechanical testing but also the equipment and materials that were employed in this investigation. Physical and mechanical tests include chemical composition, XRD, pull-off, hardness, and optical microscope analyses (SEM) and AFM . Conducting corrosion tests on the job site at the concentrated sulfuric acid plant (98%) involves two types of testing, the first for stagnation and the second for the flow of concentrated acid, as well as assessing the polarization of the samples.

3.2. Program of the Present Study

Table (3.1) represents the experimental design adopted in this study, which was obtained from the Minitab(17) program. The scheme is represented by three essential variables: the calcination temperature (500,600,700)$^{\circ}$C, the percentage of adding alumina(0,5,10)%, and the number of coating layers(1,2,3). Each essential variable has three primary levels. Figure (3.1) shows a diagram of the sequence of operations in this study, which is based on the design of the experiments.

Table (3.1):show the number of factor and variables

Variables	levels		
Temperature	500	600	700
Alumina	0	2	10
number of coating layers	1	2	3

Table (3.2): design of experiments in the Present Study

No.	**Sample code**	**Calcining temperature °C**	**no.of a layer of coating**	**AL2O3(Mol)%**
1	**S1**	**700**	**1**	**10**
2	**S2**	**700**	**2**	**5**
3	**S3**	**700**	**3**	**0**
4	**S4**	**600**	**2**	**0**
5	**S5**	**500**	**3**	**0**
6	**S6**	**500**	**2**	**5**
7	**S7**	**500**	**1**	**10**
8	**S8**	**600**	**3**	**5**
9	**S9**	**500**	**1**	**0**
10	**S10**	**700**	**3**	**10**
11	**S11**	**600**	**2**	**10**
12	**S12**	**600**	**1**	**5**
13	**S13**	**500**	**3**	**10**
14	**S14**	**700**	**1**	**0**
15	**S15**	**600**	**2**	**5**
16	**S16**	**600**	**2**	**5**

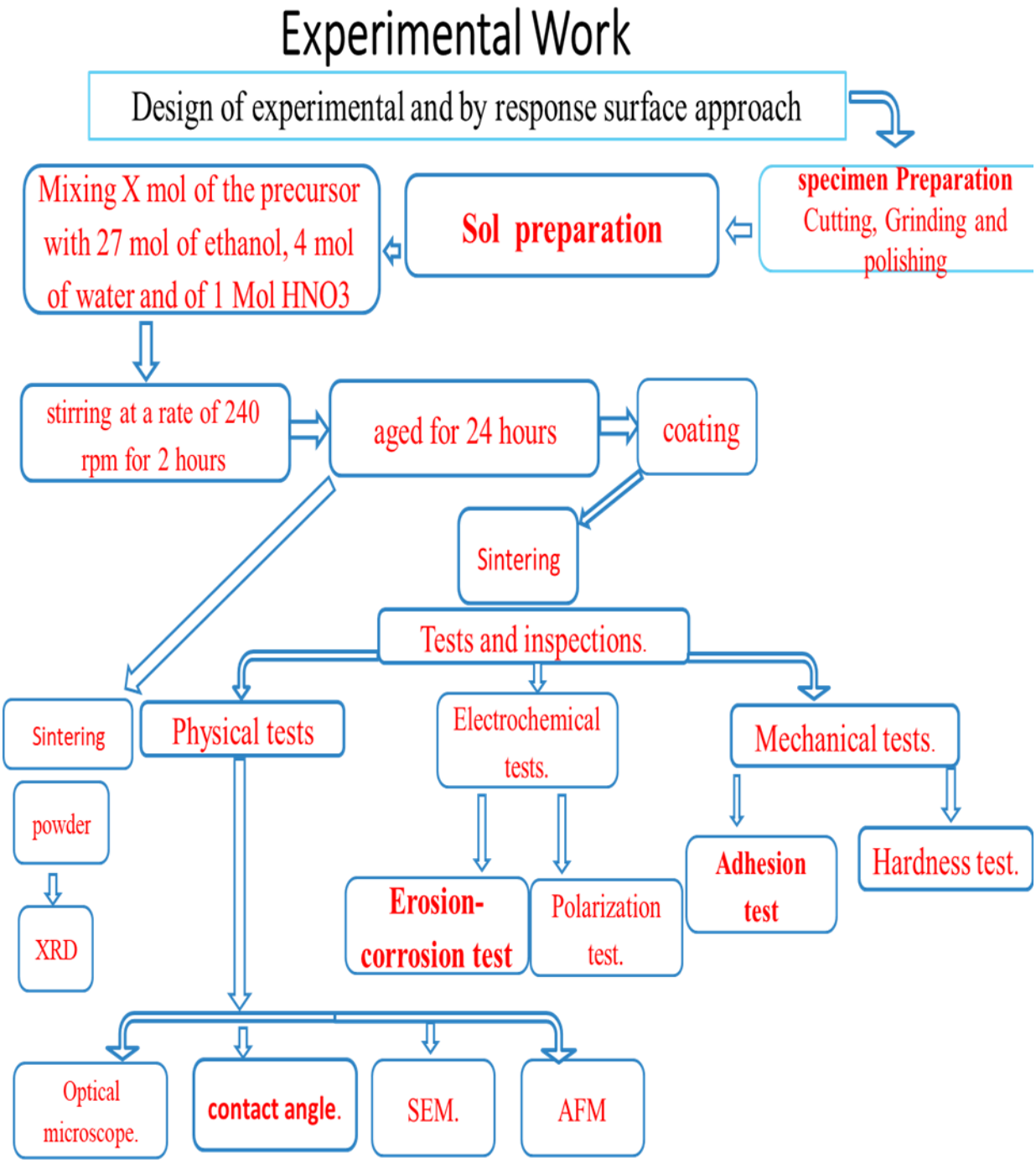

Figure (3.1): Flow chart of the experimental part of this work.

3.3. Samples Preparation

All samples were prepared at the laboratories of the metallurgical Eng. Dept. / college of Materials Eng. / the University of Babylon. The material to be coated is carbon steel obtained from Al-Furat State Company for Chemical Industries and Pesticides. Cut from a tube transporting concentrated sulfuric acid from the factory to the acid storage tanks. Table (3.3) shows the chemical composition of the sample made of carbon steel (substrate metal), and the test was carried out at a temperature of 24°C and a humidity of 20%. The examination was carried out in Baghdad at the General Company for Engineering Testing and Qualification.

Table (3.3) chemical composition of carbon steel (substrate)

Element	C%	Si%	Mn%	P%	S%	Cr%	Mo%	Ni%	Fe%
Weight (%)	**0.2**	**0.307**	**0.526**	**0.0169**	**0.0123**	**0.0251**	**0.0032**	**0.036**	**Rest**

Because of the difficulty of preparing a sample from the tubes taken, as well as the difficulty of conducting examinations for it, a steel rod with a diameter of 16 mm and a length of 100 cm and cut into samples with a thickness of 5 mm, table (3.3) shows the chemical composition of the model made of carbon steel (rod metal). We note that the chemical composition of the rod taken is similar to that of the metal from the Al-Furat Company. Afterward, mechanical methods removed the oxide layer from the samples. The sample surface is prepared with a series of emery paper (grade 320–1200). Deionized water is used to wash the samples, after which the samples are immersed in an acetone bath, and ultrasonic waves are used to remove oily spots on the surface of the samples. Then the sample are kept in

containers and covered with silica gel to prevent moisture from reaching the sample and oxidizing its surface.

Table (3 .4): Proportions of the constituent elements of metal rods

Element	C	Si	Mn	P	S%	Cr	Mo	Ni	Fe
Weight (%)	0.109	0.181	0.60	0.0085	0.0403	0.0250	0.007	0.0461	Bal

3.4 Materials used in the preparation of coatings.

Table (3.5) shows the materials used in preparing the coating material.

Figure (3.2) shows Materials used in the preparation of coatings

Table (3.5) materials used in preparing the coating material

Substance used	chemical composition	purity	manufacturer	State
Titanium(IV) isopropoxide (TTIP)	$Ti[OCH(CH_3)_2]_4$	99.999%	sigma - Aldrich	Liquid
Aluminum isopropoxide	$Al[OCH(CH_3)_2]_3$	98%	sigma - Aldrich	solid
Nitric Acid	HNO_3	60%	Jumsei chemicals	Liquid
ethanol	C_2H_5OH	99.9%	Beijing, China	Liquid
distilled water	H_2O			Liquid

3.5 Preparation of the TiO_2- Al_2O_3 Nanocomposite coating

In this work, the sol-gel method was used to prepare the coatings material at room temperature for a TiO_2-Al_2O_3 nanocomposite, based on titania, with different alumina content of 0, 5, and 10%. At first, three solutions were prepared separately, each containing a percentage of alumina different from the solution that precedes it .The method of preparing the solution is as follows: HNO_3 was mixed with ethanol to adjust the pH and then stirred with a magnetic stir for 30 minutes; then, the substance was distilled into Titanium isopropoxide (TTIP) [81]. After that, aluminum isopropoxide is dissolved in ethanol, mixed for 15 minutes, and then added to the solution in a droplet form [82]. Then the solution is kept under stirring for two hours. After that, deionized water is added to the solution to aid in the hydrolysis process and increase the polymerization process and mixed for one hour. The molar ratio varies from one solution to another. In this study, three solutions were prepared. The first solution contains only TIPP, where the molar ratio of TIPP: ethanol: H_2O:HNO_3: is 1:27:4:1. The second solution contains 5% alumina, where the molar ratio TIPP: ethanol: deionized water:HNO_3: $C_9H_{21}AlO_3$ is 0.95:27:4:1:0.05. And the third solution has 10% alumina is:0.9:27:4:1:0.1. The difference between the three solutions is the percentage of alumina, wherein the first there is no alumina, in the second 5%, and the third 10%, as shown in Table (3.5).

Table (3.5) molar ratio of the materials used in preparing the coating material.

solution number	The molar ratio of TIPP: ethanol: H_2O: HNO_3:AL_2O_3
1	1:27:4:1:0
2	0.95:27:4:1:0.05
3	0.9:27:4:1:0.1

Figure (3.2) represents a diagram of the stages of preparing solutions containing different proportions of alumina. It is divided into two stages, the first representing the creation of a solution containing only TiO_2 and the second stage containing a compound TIO_2-AL_2O_3.

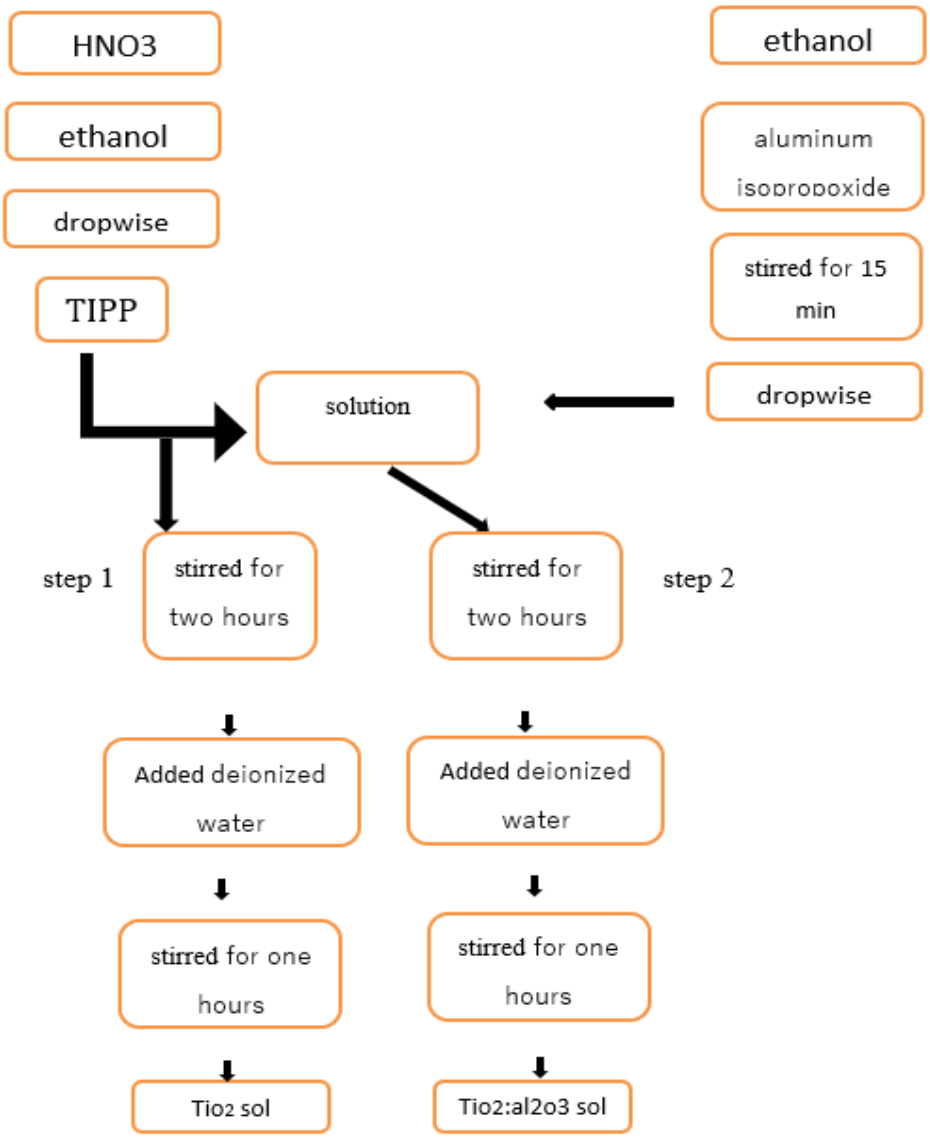

Figure (3.2): Flow chart of the stages of the synthase's sol of TiO_2, TiO_2-Al_2O_3

After the sol formation process substrate, the sol is aged for 24 hours at room temperature to leave enough time for the polymerization reactions to occur where the form of the formed gel will be white gelatinous color. Before the gel is formed, the samples are coated with Using the dip-coating device, the samples are coated in one, two, and three layers, according to the design of the experiment, as shown in Table (3.1); after the dipping process dried in a drying oven at a temperature of 80 ºC for 6 hours. After the drying process, the samples are calcined at temperatures of 500, 600, and 700 ºC for two hours at a heating rate of 5 ºC per minute according to the design of the experiment; as shown in Figure (3.4), the stages of the process of forming the film layer on the surface of the model. Figure (3.3) Shows the transformation of a sol into a gel.

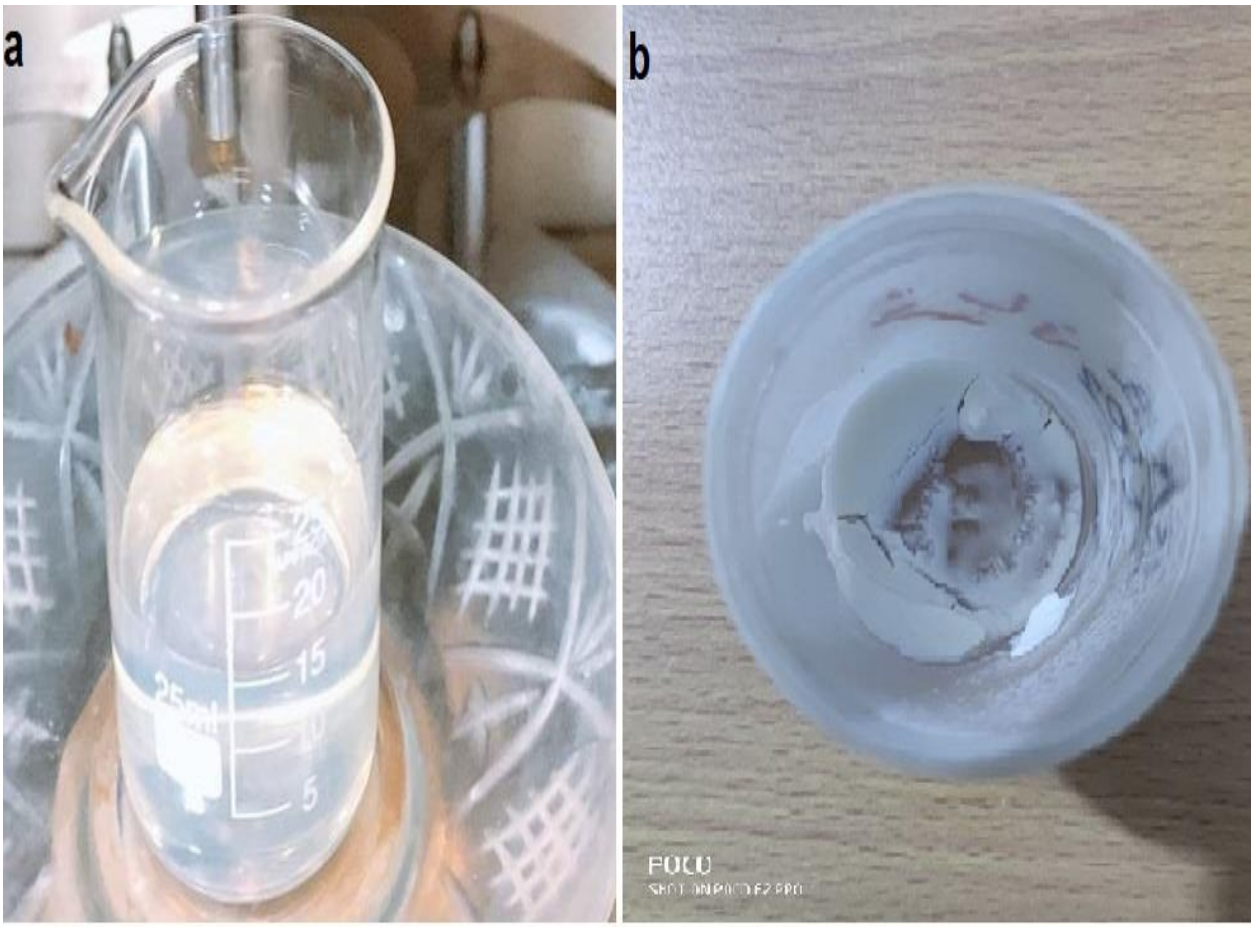

Figure (3.3). shows (a) sol ,(b) gel

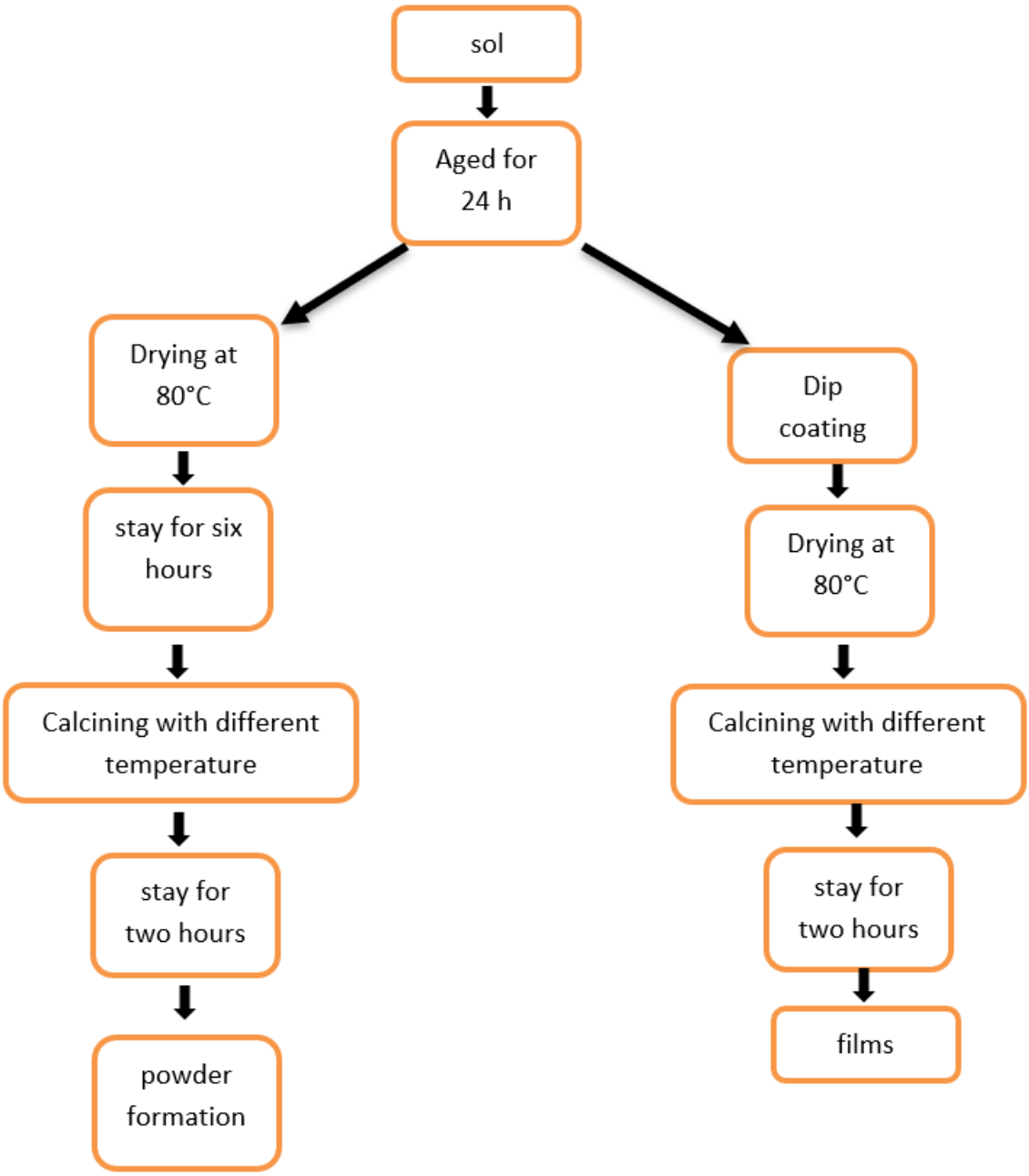

figure 3.4 (A) flow chart of (a) synthases powder of TiO_2, TiO_2:Al_2O_3, and(B) set of the preparation coating film

3.6 Preparation of the powder

The aim of preparing the powders is for the XRD examination due to the difficulty of examining coated samples, which leads to an imbalance in the readings. In this study, nine different types of powders will be prepared depending on the calcining temperature (500, 600, 700) $^{\circ}$C, as well as by relying on the design of experiments. TiO_2: TiO_2- AI_2O_3 Nanopowder was prepared via the sol-gel method using titanium tetra isopropoxide (TTIP) as the titanium source precursor, aluminum isopropoxide as the alumina source precursor, Ethanol and distilled water were used as solvents throughout the preparation process, and HNO_3 as a catalyst. Figure (3.2) A shows the schematic diagram for synthesizing TiO_2-based powder by a sol-gel method. To form a powder, first, after forming the sol, the drying process at a temperature of 80 $^{\circ}$C for six hours, followed by the calcination process at different temperatures depending on the design of the experiments for two hours, As shown in Figure (3.3), the stages of the powder formation process.

3.7 calcination

The calcination process is obtained depending on the design of the experiments and according to the temperatures (500, 600, and 700), $^{\circ}$C. Figure (3.5) shows a group of samples before and after the calcination process. When the sintering program finished, the samples were left inside the furnace to cool down till the temperature of sintered samples dropped to room temperature again.

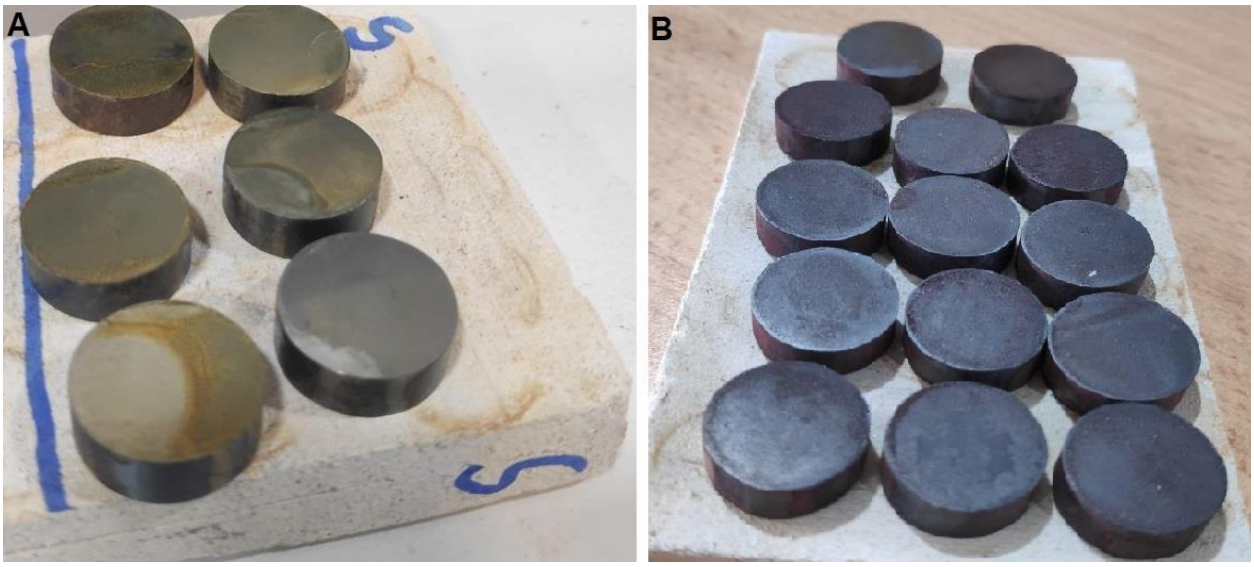

figure (3.5): (A) before calcination,(B) after calcination

3.8 dip coating

Figure (3.6) represents the dip-coating device that was used in this study with the change of many variables where the up speed was made equal to 80 mm/min, the down speed of the sample was equal to 80 mm / min and the drying time was equal to 5 seconds and the dwell time was 10 seconds. Where the test was conducted in the metallurgical engineering laboratories of the University of Babylon in the device (PTL-OV6P Dip coater)

Figure (3.6). shows a dip coating

3.9 Tests and inspections

Most tests were done at the laboratories of Materials Eng. Labs. /

University of Babylon and TU Berg Akademie Freiberg , Germany

3.9.1 1 inspection

3.9.1.1 X-ray Diffraction (XRD)

Ku X-Ray generator that was employed, and it produced Cu K radiation at 40KV and 20mA. The X-ray is produced using a general electric diffractometer of the Philips (PW 1840) type, which scans at a speed of six degrees per minute. During this process, the detector was rotated across an angle that ranged from 0 to 80 degrees. At the General Company for Examination and Rehabilitation Engineering in Baghdad, the XRD analysis was conducted out. To order to identify the phases of both the matrix phase and the reinforced particles, X-ray diffraction was used, and then those phases were compared to the standard charts.. From x-ray diffraction, peak Crystallization size is measured by the Scherrer equation.

$$D=k\lambda/\beta \cos \theta$$

by using full width at half-maximum (FWHM)of the (101) 2θ anatase peak at 25 (D) is the crystallite size k is a constant(k=0.89), λ is the Cu Kα X-ray wavelength (1.5406Å), and β is the FWHM of the 2θ peak. The Scherrer equation was calculated using the program (x peart).

Figure (3.7): X-ray diffraction machine

3.9.1.2 Scanning Electron Microscope (SEM)

The scanning electron microscope examination was used to reveal the microstructure of the optimum samples after sintering. The test was carried out _ by using SEM type (inspect S50).

3.9.1.3 Optical Microscope Analysis

The Microstructure of the coated samples has been tested by an optical microscope lab in Germany / Freiberg (TU Berg Akademie) by (optical microscope, model Metallux 3) as shown in figure (3.8). The coated samples are cleaned with ethanol, air dried, and examined using a light microscope.

Figure (3.8). optical microscope

3.9.2 mechanical tests

3.9.2.1 nanoindentation test

A typical nanoindentation experiment involves the indenter making contact with the coating's surface and penetrating it to a certain depth or load. The indenter's penetration depth into the coating layer, which has been set at 500 nanometers, is thought of as a sample displacement. The hardness value is determined as shown in the following equation[83].

$$H = \frac{\text{Pmax}}{\text{A}} \quad \ldots\ldots \ldots\ldots\ldots 1$$

Equation (1) illustrates how to calculate the hardness H of a material by dividing the maximum load Pmax by the predicted contact area A of the indenter at maximum load. Figure (3.9) A shows a diagram of the indenter penetration into the coating layer, the projected contact area, A, can be determined from the contact depth h_c at maximum load P_{max}, such as in Equation (2) [83].

$$A = C_0 h_c^2 \quad \ldots\ldots\ldots\ldots\ldots\ldots 2$$

The indenter tip affects the value of C_0. For example, the Perkovich pyramidal diamond tip's value of C_0 is 24.5. In the international standards to test the sample and take the sites of contact of the indenter with the surface of the sample according to the scheme, Where nine sites of contact with the sample surface are taken for testing. Figure (3.9) B shows the locations of taking the hardness value to the one sample and taking the average hardness value.

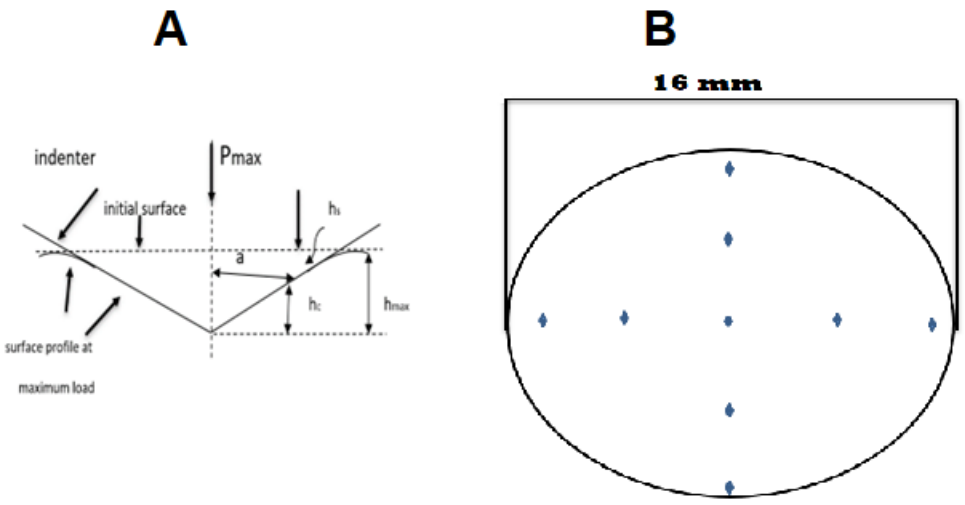

figure (3.9). (A)diagram of the indenter (B) test-taking points

3.9.2.*2* Pull-Off Adhesion Test

The pull-off test is the most common test for the adhesion of a coating to a base metal surface. Before conducting the test, the sample's surface is thoroughly cleaned with ethanol to remove any deposits of fats and oils for the best bonding between the test kit and the surface. The test tool, usually called a dolly, as shown in figure (3.10), is attached to the coating surface by an adhesive substance called glue. Moreover, using the retractable stacking device, the load increases

continuously and equals 100% in all test areas. As the forces required to pull the dolly or the forces that the dolly bears result in a tensile strength per square inch (psi) or megapascals, the readings are recorded for all samples.

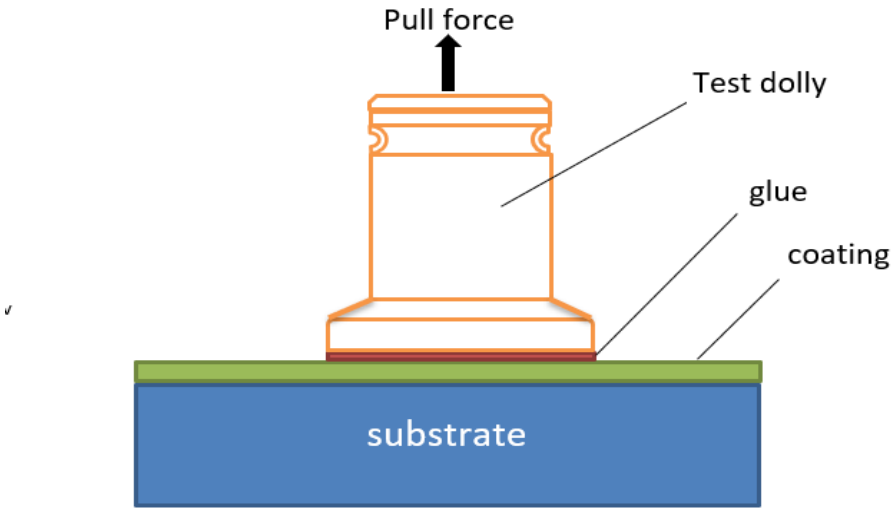

Figure (3.10): diagram of the dolly and substrate

3.9.2.*3* Measurements of coating thickness

For non-destructive examination of coating layers on the surface of the substrate. The thickness of the coating layer was examined in the Department of Polymer Engineering and Petrochemical Industries/College of Materials Engineering-University of Babylon by using(Digital Coating Thickness Gavage (TT260)), where the thickness of the coating layer was measured. For six sit in the surface for each model, the average thickness of the layer was extracted. As shown in figure (3.11).

Figure (3.11): The device of thickness measuring

3.9.2.*4* Contact Angle Measurement

The static contact angle (θ) of a droplet on a solid surface, which is an important index to quantitatively evaluate the wettability of a solid surface, was used to measure the hydrophobicity or wet-ability of the coated layer sample samples. The optical contact angle equipment type CAM 11O-O4W that was attached with the CCD camera was used to measure contact angle. The droplet was placed on the solid surface, and then the contact angle was measured. Each contact angle was measured five times between each test liquid and each solid surface in the separate tests, and ten measurement sites were chosen. As seen in figure (3.12), the test was conducted at the TU Berg Akademie Freiberg in Germany.

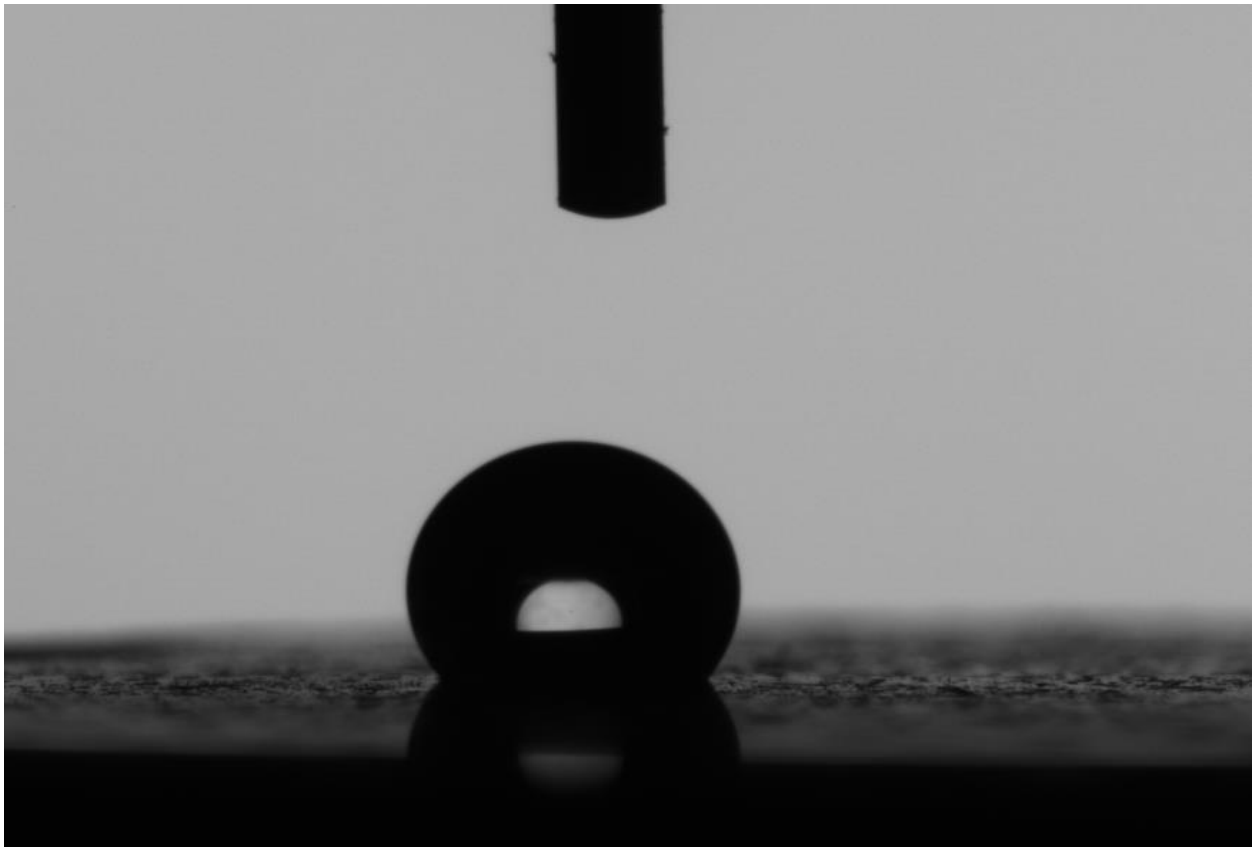

Figure (3.12) show a Contact Angle

3.9.3 Corrosion Test

3.9.3.1 Electrochemical (potentiodynamic polarization) test

This type of examination includes the electrochemical test of the corrosion rate based on the extraction of the value of the corrosion current and the corrosion potential difference for the samples under examination. Experiments in electrochemistry were carried out in three-electrode cells that contained electrolytes (500 ml) in the form of a solution of concentrated sulfuric acid; the counter electrode was the Pt electrode, the reference electrode was SCE, and the working electrode (specimen) was determined in accordance with the standards established by the American society for testing and materials (ASTM) G102-89 [84] . After plotting the potentiodynamic polarization curves, both the corrosion

current density (Icorr) and the corrosion potential were determined by employing anodic and cathodic branches in Tafel plots. After starting with a voltage that was 250 mV below the open circuit potential, the test was carried out by gradually increasing the potential at a scanning rate of 0.4 mV per second. The scan went on for as much as 250 mV beyond the voltage of an open circuit. Using the equation, we can determine the amount of corrosion that has occurred in the samples.

Pi = 22.85 icorr …….(3) [85]

where Pi (Corrosion rate)

Figure (3.13): polarization test

3.9.3.2 Erosion-corrosion test in concentrated Sulfuric acid

According to ASTM (G73), this test was carried out at Al-Furat State Company for Chemical Industries and Pesticides. This test, which is the opposite of the immersion test, involves exposing the samples to the effect of erosion-corrosion on the surface of the metal as a result of the movement of the concentrated acid. This test examines the behavior of the metal as a result of the acid mass impact on the surface as a

physical action of movement combined with the chemical effect of the acid as a corrosive medium. The existence of a tube to transmit concentrated acid from the factory to a tank, which is used to assess the degree of erosion-corrosion resistance of the samples, is essential to the testing process. The characteristics of the acid that is moving through the conveying tubes are outlined in the table (3.6). where the same procedures are used to calculate the corrosion rate when the object is submerged. The procedure for carrying out the test at Al-Furat Company is shown in figure (3.14).

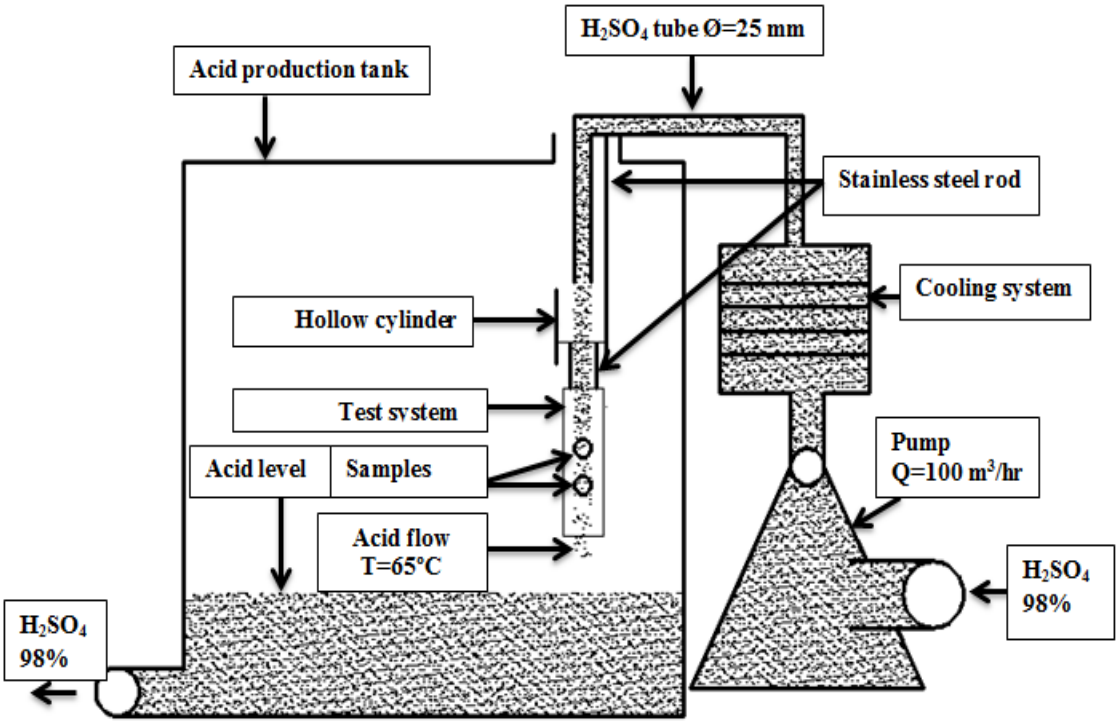

Figure (3.14): Diagram showing the mechanism of the (Erosion -corrosion) Examination

The steps for this test are as below:

1. A determination of the sample's starting weights will be made (W_0). In order to attain high weight accuracy, a sensitive balance capable of high precision with four decimal places was used.

Table (3.6) properties of H_2SO_4 in the pipe

Tube diameter	(25) mm
flow rate	10 (m s^{-1})
Temperature	65(°C)
density of acid	(1.84) kg/m^3

2. Immerse the samples in concentrated sulfuric acid (98%) for a specified period

3. After the allotted of time has elapsed in the water, the samples are removed, washed with water that has been distilled, and then dried in an electric oven at a temperature of 65 degrees Celsius for one hour.

4. Calculate the weight difference between the original weight and the new weight after immersion by measuring the weight after immersion (W1) and then subtracting the initial weight from the new weight after immersion.

5. The corrosion rate is calculated by the weight loss method according to the equation (4): [86]

Corrosion rate = $\frac{\Delta W}{t.A}$ …….(4)

ΔW: It represents the difference in weight between the starting weight (W_0)

and the weight after immersion (W_1), equal to (W_0-W_1).

A: Acid-exposed surface area (cm^2).

t: Acid exposure time (day).

Chapter

4

Results and Discussion

Chapter Four

Results & Discussion

4.1. Introduction

The fourth chapter reviews and discusses the results of this study's physical and mechanical tests. The results were discussed in the framework of various aspects, choosing the optimum percentage of alumina in the coating material, the annealing temperature, the number of coating layers, and its effect on the mechanical and chemical properties.

4.2. Results of Physical and Mechanical Tests

4.2.1. X-Ray Diffraction Analysis

X-ray diffraction analysis of synthesized TiO_2 and TiO_2:AL_2O_3 powder prepared by sol-gel at various sintering temperatures based on the formula adopted in this study was sufficient to produce crystalline TiO_2 as shown in figure (4.1). The diffraction peaks of all powder are attributed to the anatase phase of TiO_2 (JCPDScard no. 21-1272). There was no indication of the rutile phase. Relying on previous studies, the transformation temperature from anatase to rutile is 760 ºC [87].To study the effect of heat treatment on the crystallinity of a group of powders sintering temperature as demonstrated in table (4.1). Increasing the heat treatment leads to an increase in the crystallinity, and the reason for this may be attributed to the rise in temperature that leads to an increase in the transformation of the substance from amorphous to a crystalline substance and approaching the transition to the rutile phase. In addition, the addition of alumina affects crystallinity, as it leads to an increase in the rate of crystallinity, as shown in Table (4.1). It is worth noting that the crystallite size was estimated by using Scherer's

equation from the (101) peak of anatase TiO_2, as demonstrated in table (4.1). It is noted that the calcination temperature and the addition of alumina affect the crystallite size, as increasing the proportion of alumina leads to a decrease in the crystallite size, as well as the temperature increase, the crystallite size increase [88].XRD peak broadening analysis for TiO_2:Al_2O_3 powder at different temperatures and different volume ratios of AL_2O_3 show that any peak related to the alumina crystal phase was not observed due to inadequate heat treatment temperature for alumina crystallization. In previous studies, it appears that the alumina crystallizes at a temperature of 900 ºC; below this temperature, it remains amorphous [76].

Table (4.1) Crystallization ratio and crystallite size analysis of XRD test

No.	Sample cod	Temperatures Cº	Al_2O_3 Mol %	Crystallization %	crystallite size n.m
1	A1	500	0	36.53	10.3
2	A2	600	0	52.7	15
3	A3	700	0	61.33	27.2
4	A4	500	5	46.61	9.8
5	A5	600	5	59.44	12.7
6	A6	700	5	60.48	17.4
7	A7	500	10	45.03	9.3
8	A8	600	10	54.9	11.6
9	A9	700	10	64.21	14

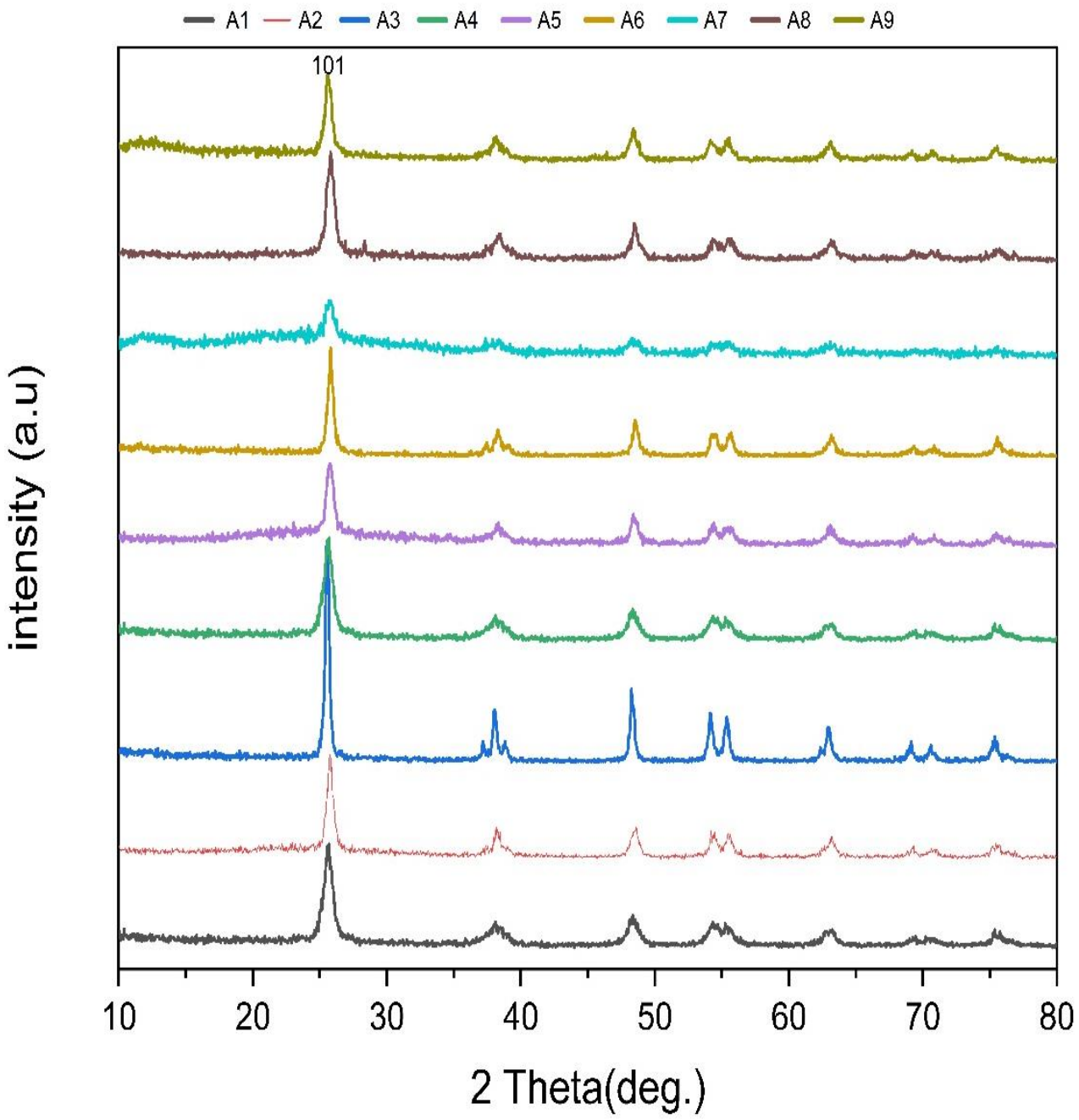

Figure (4.1) XRD patterns of all sample

The peak position at 2θ (25.6) was dominant with much higher intensity Than other peaks. As the annealing temperature was increased from 500 to 700 ºC, peak intensity and crystallization ratio gradually increased. In Figure (4.1), the

XRD analysis of a group of powders by adding different percentages of alumina shows that increasing the rate of AL_2O_3 leads to a decrease in the intensity of the peaks.

4.2.2. Optical Microscope Analysis

The surface morphology of the polished low carbon steel and the applied coating layer developed based on the design of experiments are demonstrated in figure (4.2). It was noted that the polished steel that does not contain a coating layer as in Figure (4.2) S0 has grooves and lines formed during the grinding process. The presence of these lines and grooves has a benefit for coating as it leads to a mechanical interlocking between the coating layer and the surface of the base sample. After applying the coating to the model, it can notice that the grooves and lines have disappeared, indicating the coating layer's homogeneity. We can see that increasing the temperature from 500 to 600 ºC improves the morphology and reduces the number of pores and cracks, but when the temperature increases to 700 ºC, we notice that the samples have many defects due to a difference in the thermal expansion coefficient between the coating layer and the base metal., which leads to the expansion and contraction between the metal and the coating. This leads to cracks appearing, as shown in figures (4.1) S1, S2, S3, S10, and S14. In addition, it was observed that the effect of the thermal expansion coefficient is more negligible under this temperature 700 ºC, as shown in figure (4.2) S4, S5, S 6, S7, S8, S 11, S12, S1 3, S15. Another factor affecting the morphology is the number of layers. Thin films can be obtained for the coating from a few layers. However, it was observed that the thickness of the thin layer and the surface defects increase with the increase in the number of dipping. It can also be observed that increasing the thickness of the coating layer leads to the appearance of micro cracks, especially at high temperatures as in S10, S3, and S2. It has also been observed that increasing the percentage of alumina from 5% to 10% is a clear improvement in the

morphology and makes it more homogeneous. It is also possible to compare between coating layers containing alumina and non-containing under the same conditions of temperature and number of coating layers, as in figure (4.2). Compared, it can be seen that samples containing alumina better reduce coating defects. This is because alumina minimizes the size of the surface pores of the samples and reduces micro cracks[79].

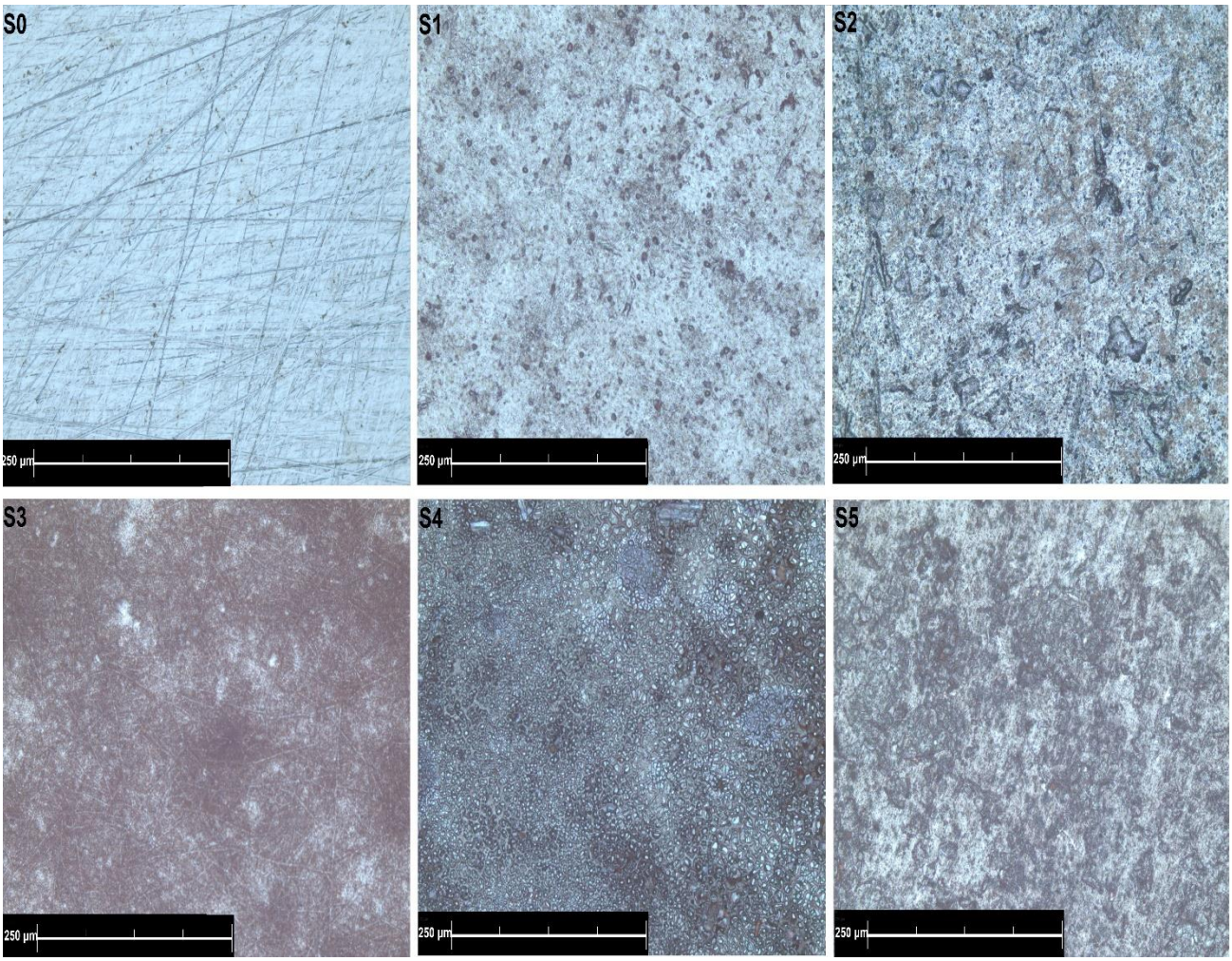

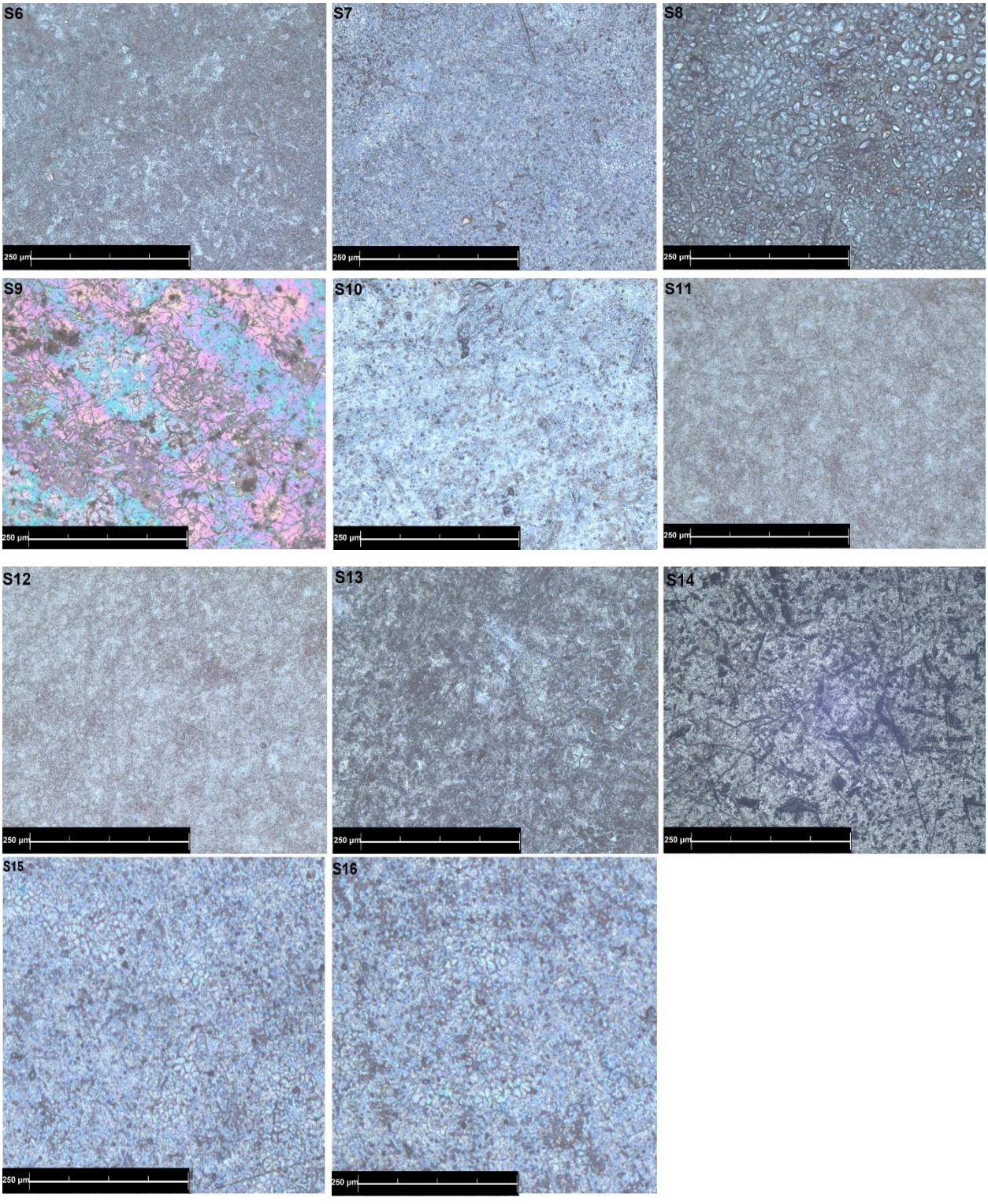

Figure (4.2) Optical micrographs of the surface

4.2.3 Thickness test

In general, the thickness of the films increases with the number of layers. Figure (4.3) Shows the effect of each of the variables (temperature, number of layers, and alumina content) on the thickness of the coating layer. From the results, it can be seen that the consistency of the one-layer ranges between: 1.03-1.61 μm, the second layer is 1.73-2.29 μm, and the third layer is 2.5-2.7 μm; this means that the number of layers has the most significant effect on the thickness. It can also be noted that the value of the thickness of the coatings layer when coating with multiple layers is not constantly incinerating to the coating layers' defects. Table (4.3) shows the results obtained for the coating thickness test. The results show that increasing the temperature decreases thickness due to the reduction of defects, where the coating material spreads homogeneously [89]. Table (4.2) shows the results of the ANOVA analysis for thickness. The analysis of variance for the factors affecting the thickness of the TiO_2 - based coating layer shows the percentage of contribution (cont.) of each term of the models. The results showed that the most significant influencing factor is the number of layers, which affects by a percentage of 85.9%, and the contribution percentage of temperature and alumina is 10.4% and 3.1%, respectively.

The probability value for all coating process factors (temperature, number of layers, and alumina content) is ($p<0.05$), indicating that (temperature ($p=0.0008$), no. of layer ($p=0.0001$,) and alumina content ($p=0.0083$) which showed have a significant impact on the thickness of the coating layer.

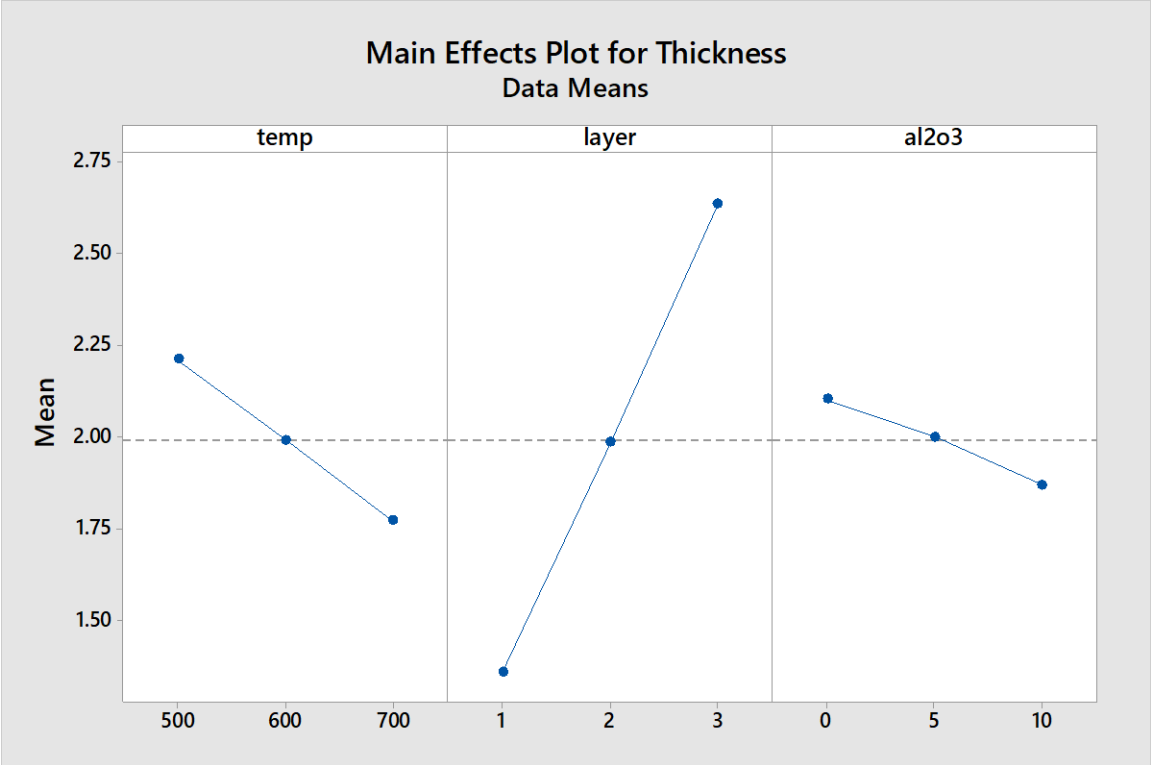

Figure (4.3) The effects of temperature, alumina content, and the number of layers on thickness.

Table (4.2): ANOVA Results for thickness

Source	Sum of Squares	df	Mean Square	F-value	p-value
Model	4.73	9	0.5252	99.38	< 0.0001
A-Temperature	0.4884	1	0.4884	92.42	< 0.0001
B-no. of layer	4.08	1	4.08	772.62	< 0.0001
C-AL2O3	0.1369	1	0.1369	25.90	0.0022
AB	0.0066	1	0.0066	1.25	0.3061
AC	0.0078	1	0.0078	1.48	0.2697
BC	0.0015	1	0.0015	0.2862	0.6119
A^2	0.0000	1	0.0000	0.0043	0.9499
B^2	0.0014	1	0.0014	0.2623	0.6268
C^2	0.0019	1	0.0019	0.3655	0.5676
Residual	0.0317	6	0.0053		
Cor Total	4.76	15			

Table (4.3) shows the results obtained for all tests

No.	S.C	Temp C	N.O.L	AL2O3 mol	Adhesion MPa	Hardness GPa	Thickness μm	corrosion rat mm y-1	Icorr (μA/cm2)	Ecorr (mV/SCE)	Erosion-corrosion rat
1	S1	700	1	10	25.1	8.826	1.03	0.457	18	-197.7	0.0003 7
2	S2	700	2	5	22	8.238	1.73	0.6169	27	-257.2	0.00028
3	S3	700	3	0	15.3	6.963	2.5	0.914	40	-320	0.0004
4	S4	600	2	0	27.01	6.639	2.17	0.1713	5.2	-165	0.00007 8
5	S5	500	3	0	20.2	6.1	2.91	0.1828	8	-178	0.00012
6	S6	500	2	5	23.1	6.473	2.29	0.1371	4	-139.1	0.00007 5
7	S7	500	1	10	36	7.375	1.45	0.3427	5	-158.3	0.0002
8	S8	600	3	5	28.4	6.669	2.69	0.3656	14.2	-190	0.00013
9	S9	500	1	0	28.3	4.413	1.61	0.3884	9.8	-180	0.00022
10	S10	700	3	10	22.23	9.1	2.27	0.7540	33	-290	0.00037
11	S11	600	2	10	33.11	8.14	1.79	0.0502	2.1	-140	0.00002 5
12	S12	600	1	5	40.6	7.041	1.37	0.1828	3	-153	0.00011
13	S13	500	3	10	25.21	7.77	2.8	0.1530	6.5	-160	0.00008
14	S14	700	1	0	18	6.865	1.32	0.6580	21.1	-210	0.00033
15	S15	600	2	5	32.4	7.29	1.91	0.139	5.3	-155.2	0.000057
16	S16	600	2	5	32.2	7.3	2.01	0.147	5.1	-167.5	0.0000575

4.2.4 Pull-off testing

The results of the adhesion test of the various samples base on the design of the experiment are listed in the table (4.3). Statistical analysis showed that the annealing temperature is the predominant factor affecting the adhesion level (Cont. 49.18%), while the multi-layer coating is the second factor (Cont. 18.2%). At the same time, alumina content has the lowest effect on adhesion level (Cont. 13. 9%). The coating layer's tensile bonding strength gradually increases when the temperature rises from 500-600 [90].as the tensile strength value increases from 23 to 40 MPa, as shown in the drawing main effect plot Figure (4.4). In addition, the results showed that an increase in the temperature to 700 º C Significant decreases adhesion resistance values because of the difference in the coefficient of thermal expansion between the base metal and the coating layer. This leads to the appearance of many micro-cracks on the surface, which act as centers for the localization of stresses on the surface, leading to a decrease in adhesion values. It has also been noted that the diversity of layers from one layer to three layers has a negative effect on the adhesion resistance, as increasing the number of layers to three gives the lowest adhesion value. The reason for this is that the increase in thickness leads to the appearance of cracks on the coating layer [91].In this work based on experimental design, it was found that increasing the percentage of alumina from 0 to 10% effectively affects adhesion. This is due to the modification of microstructure as it makes the coating layer more dense due to blocking the pores and microcracks that occur in the coating. Figure (4.4) shows the matching between the experimented and predicted values for each response.

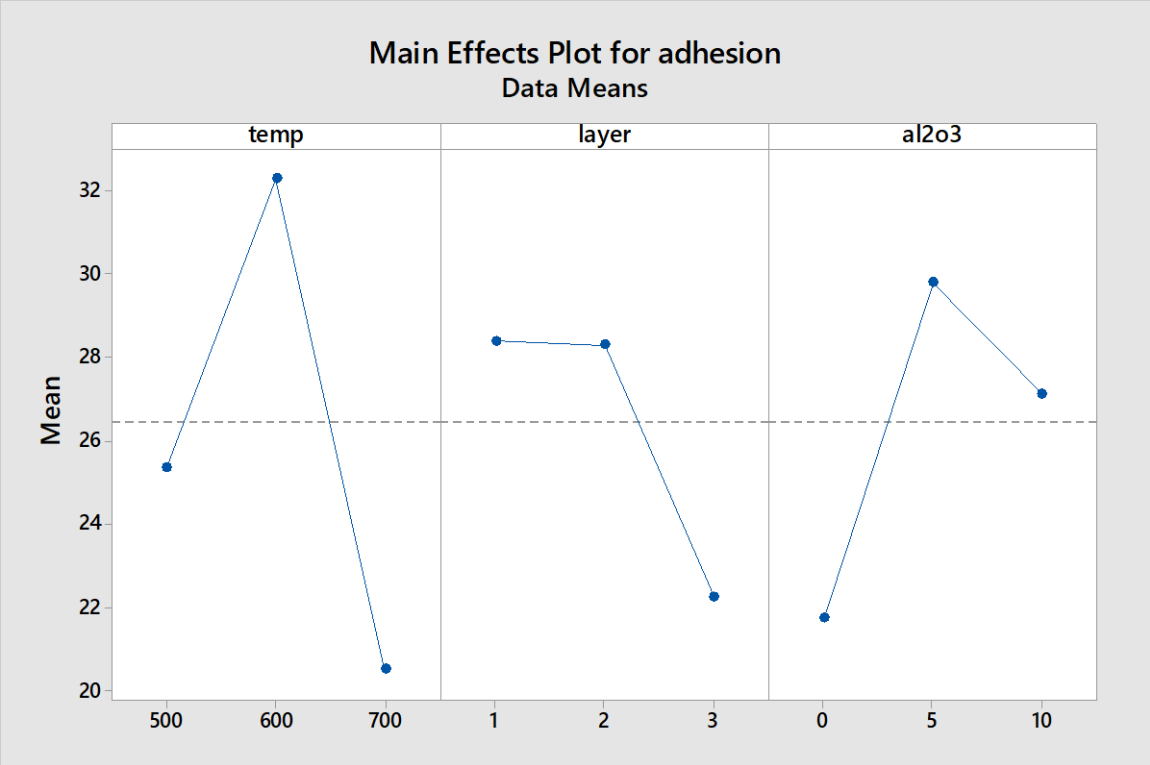

Figure (4.4) The effects of temperature, alumina content, and a number of layers on adhesion.

Table (4.4): ANOVA Results for adhesion

Source	Sum of Squares	df	Mean Square	F-value	p-value
Model	586.48	9	65.16	11.61	0.0037
A-Temperature	58.47	1	58.47	10.41	0.0180
B-no. of layer	94.00	1	94.00	16.74	0.0064
C-AL2O3	72.04	1	72.04	12.83	0.0116
AB	6.70	1	6.70	1.19	0.3166
AC	6.70	1	6.70	1.19	0.3166
BC	1.23	1	1.23	0.2195	0.6559
A^2	239.42	1	239.42	42.65	0.0006
B^2	15.44	1	15.44	2.75	0.1483
C^2	10.75	1	10.75	1.92	0.2156
Residual	33.68	6	5.61		
Cor Total	620.17	15			

4.2.5 Nano hardness test

Table (4.3) shows the hardness values of the coating films on low carbon steel obtained from nanoindentation tests. The results showed that the hardness of the base metal is 2.148GPa. Table (4.5) shows the results of the ANOVA analysis for Nano hardness. The same table can show the percentage of contribution for each variable. From the analysis, it can be seen that the effect of adding alumina is 49.96%, the percentage the effect of temperature is 37.3%, and the percentage of the effect of the number of layers is 8.26%. The hardness increases with the increase in the calcining temperature from 500 to 700 ºC. The coating has porosity, as a high degree of calcination leads to a reduction in the porosity size, which leads to an increase in the density of the coating and an increase in its hardness. It is also possible to notice that adding alumina has a positive effect on the hardness, as the hardness increases by a significant amount due to the disappearance of many defects, including porosity and micro-cracks, as we showed in the microscope test [92]. The results of the light microscope showed that adding alumina affects the structure, making it more homogeneous because the alumina leads to closing the pores resulting from coating defects and liberating organic materials during the calcination treatment. It was also noted that an increase in the number of layers has Less effect on hardness, as an increase in the number of layers means an increase in the density of the coating. This can also be clarified as the layer defects such as porosity and cracks can be erased by the subsequent layer. This positively affects the hardness as it has a negative effect. Also, by increasing the number of layers, micro-cracks appear in the last layer of the coating, which leads to a decrease in the hardness value [93].effect of the three variables can be shown in figure (4.5), which represents the main effect plot.

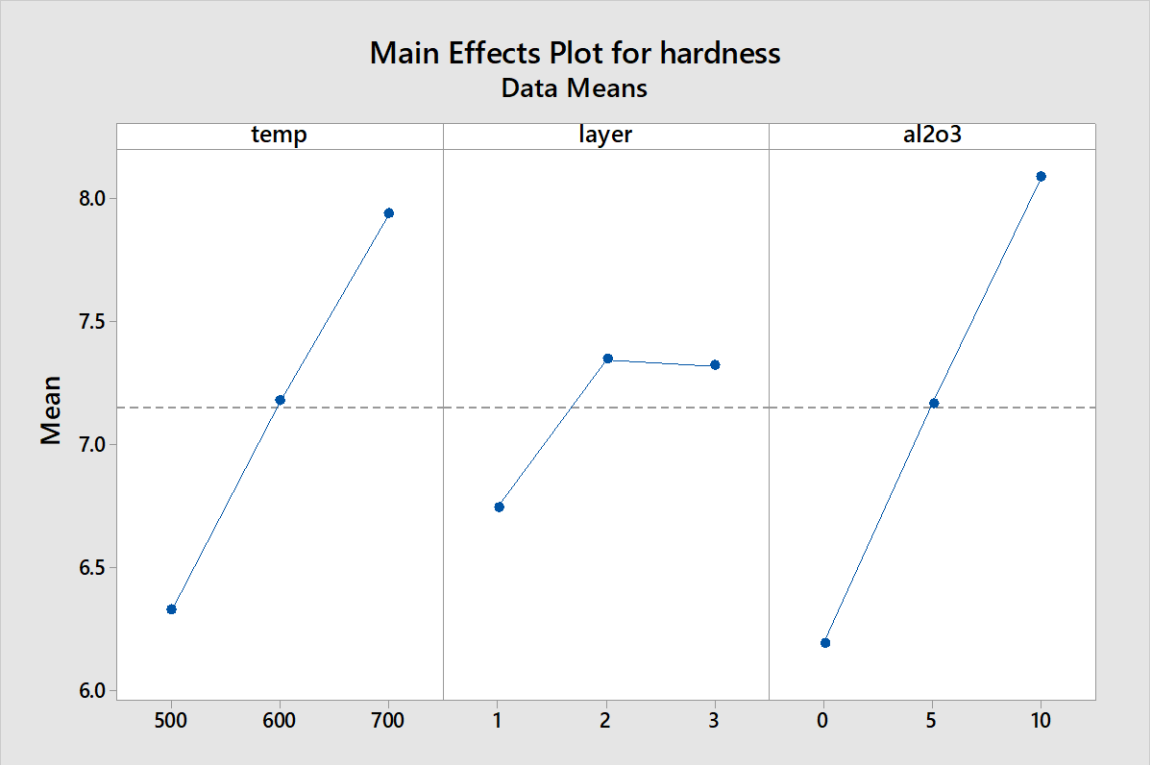

Figure (4.5) The effects of temperature, alumina content, and a number of layers on hardness.

Table (4.5): ANOVA Results for hardness

Source	Sum of Squares	df	Mean Square	F-value	p-value
Model	17.14	9	1.90	13.03	0.0027
A-Temperature	6.46	1	6.46	44.16	0.0006
B-no. of layer	0.8162	1	0.8162	5.58	0.0561
C-AL2O3	8.94	1	8.94	61.15	0.0002
AB	0.4442	1	0.4442	3.04	0.1320
AC	0.0161	1	0.0161	0.1102	0.7512
BC	0.0145	1	0.0145	0.0994	0.7632
A^2	0.0210	1	0.0210	0.1438	0.7176
B^2	0.4457	1	0.4457	3.05	0.1314
C^2	0.0401	1	0.0401	0.2741	0.6193
Residual	0.8773	6	0.1462		
Cor Total	18.02	15			

4.2.6. Potentiodynamic polarization

Figure (4.6) shows the polarization curve of different coatings based on the design of experiments using a potential dynamic polarization test. Corrosion potential (Ecorr) and corrosion current density (Icorr) were obtained from polarization curves using the Tafel extrapolation method. Low carbon steel, the base metal in this study, showed the value of the corrosion current density (Icorr) and corrosion potential (Ecorr) 179 μA/cm2, -507 mv sequentially when exposed to an acidic solution of H_2SO_4 at a concentration of 98%. Corrosion potential and corrosion current density of coated samples are shown in table (4.3). The higher i corr value of low carbon steel sample compared to all samples coated with different TiO_2 base coating nanocomposite thin films suggests the passive nature of the ceramic coating. The presence of TiO_2-based coating shifts the polarization diagram to values of less corrosion current density and more noble potentials, i.e., the presence of TiO_2-based coating thin film improves the corrosion resistance of Low carbon steel substrate in 98% H_2SO_4 solution. It is well known that the quality of the coating has an essential effect on corrosion behaviour; the high quality of the layer, which shows few structural defects, as shown in Figs (4.1) S11, S7, contributes to good corrosion resistance. It has been observed that the micro crack is the most critical factor affecting corrosion resistance. Samples coated with micro crack structures showed a higher corrosion rate than those without cracks. The electrochemical reaction takes its course, which leads to an increase in the density of the corrosive current. In the microstructure, we show that the coatings that did not exhibit this electrochemical behaviour are more dense, and the micro-cracks are few, which leads to the release of metal ions and their exit to the surface and thus severe corrosion of the base metal. It was observed that increasing the temperature from 500 to 600 ºC improves the microstructure and reduces the number of pores and cracks, as in S11 and S7, but when the temperature increases

to 700 ºC, It was noted that the samples have many defects due to a difference in the thermal expansion coefficient between the coating layer and the base metal as in S1. Through the results, we note that the samples treated with a temperature of 700 ºC suffer from a high corrosion rate compared to the samples treated at the temperatures of 500 and 600 ºC, This is due to the layer being homogeneous, and the presence of micro cracks was not observed at low calcination temperature. On the other hand, the presence of AL_2O_3 in the coating increased the density and homogeneity of the coating. This can be seen in the table (4.3), which leads to a decrease in the corrosion current value and a reduction in the corrosion rate for samples containing alumina. The ANOVA table (4.6) shows that temperature has the most significant effect, as its contribution ratio is 68.5 % due to its influential role in stimulating the formation of cracks. It can be seen that the percentage of the effect of the multi-layering of the coated samples is 13.5%, as the increase in the number of layers to three leads to the appearance of micro cracks, and as we mentioned previously, its effect, which is noticed through the table (4.3) an increase in the corrosion current and an increase corrosion rate. At the same time, the percentage of alumina contribution is less than that, about 3.8%. The information related to the polarization test proved that the nanocomposite TiO_2 + Al_2O_3 is suitable for corrosion resistance and can be placed in an environment of H_2SO_4 acid. Figure (4.7) represents the main effect plot.

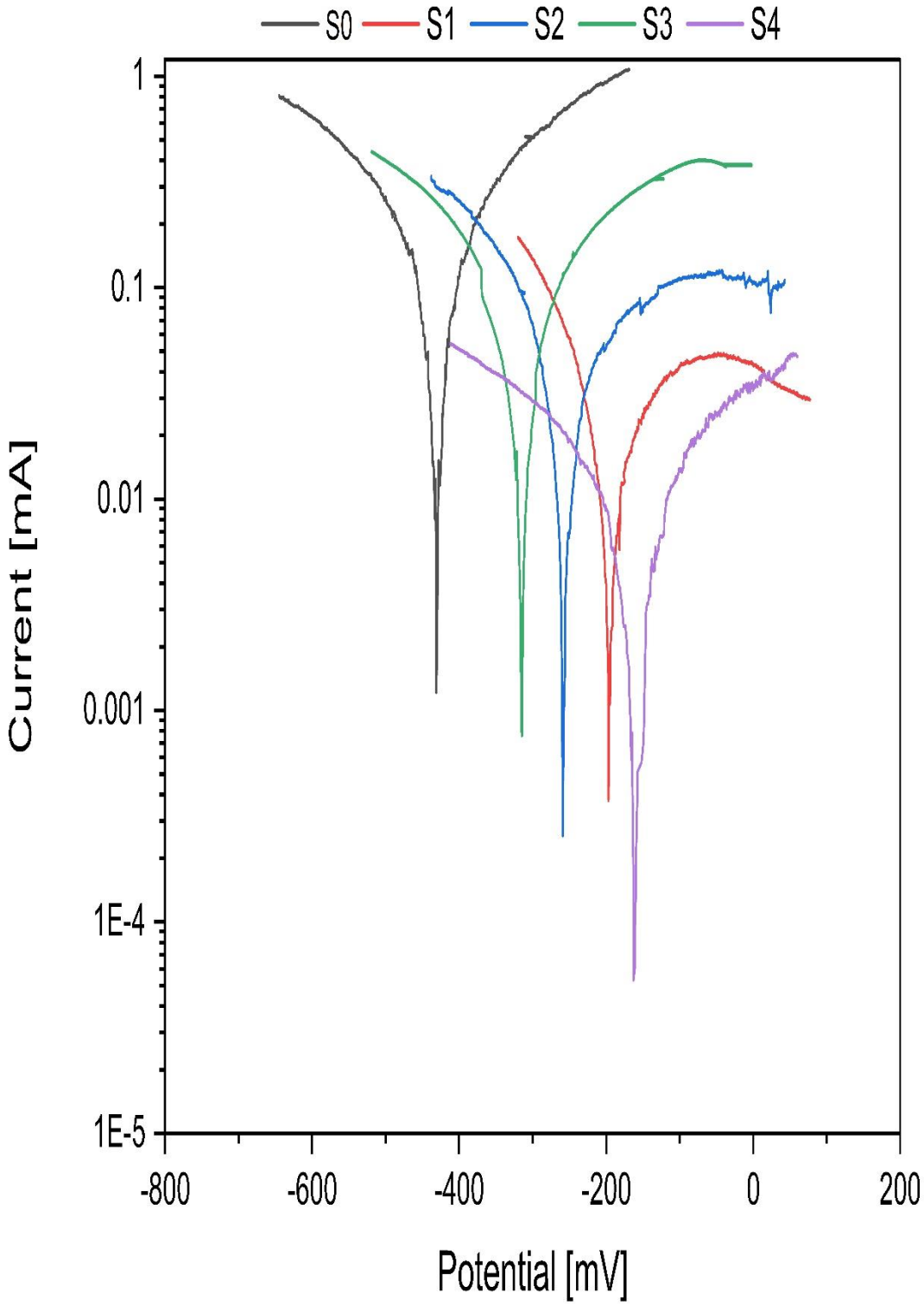
S0
S1
S2
S3
S4
1
0.1
0.01
0.001
1E-4
1E-5
Current [mA]
-800
-600
-400
-200
0
200
Potential [mV]

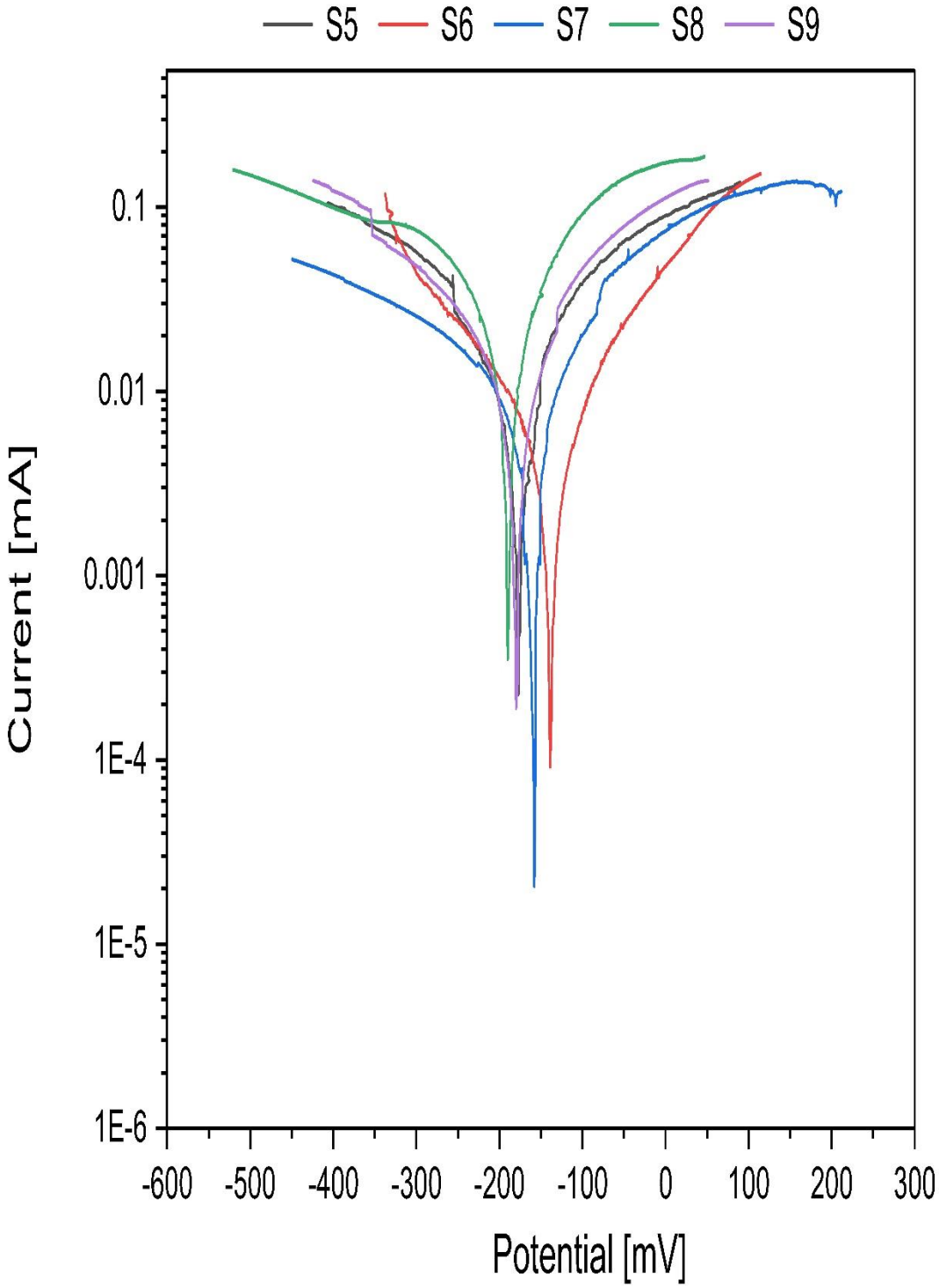
S5
S6
S7
S8
S9
0.1
0.01
0.001
1E-4
1E-5
1E-6
Current [mA]
-600
-500
-400
-300
-200
-100
0
100
200
300
Potential [mV]

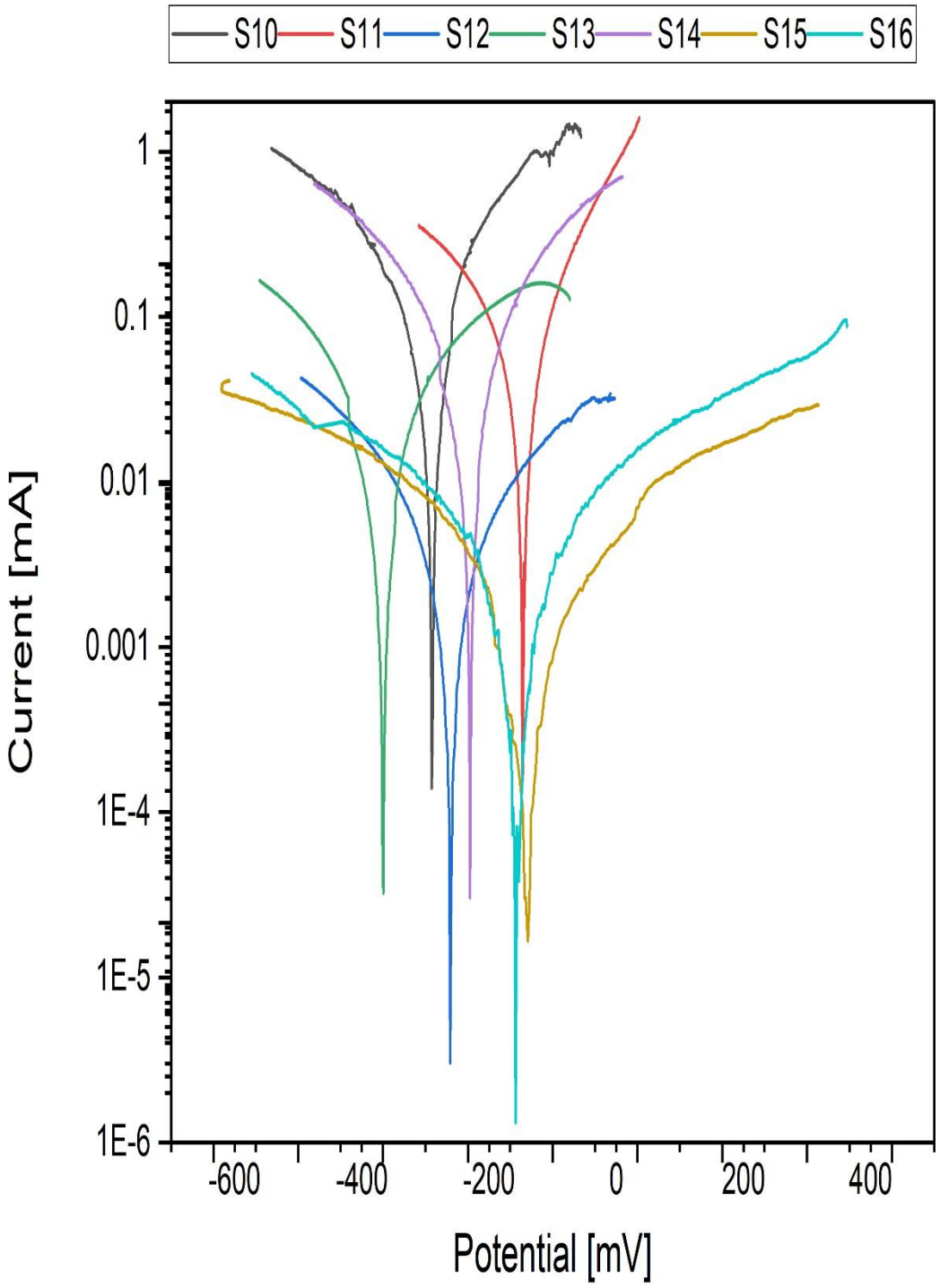

Figure (4.6): Polarization curve of all sample

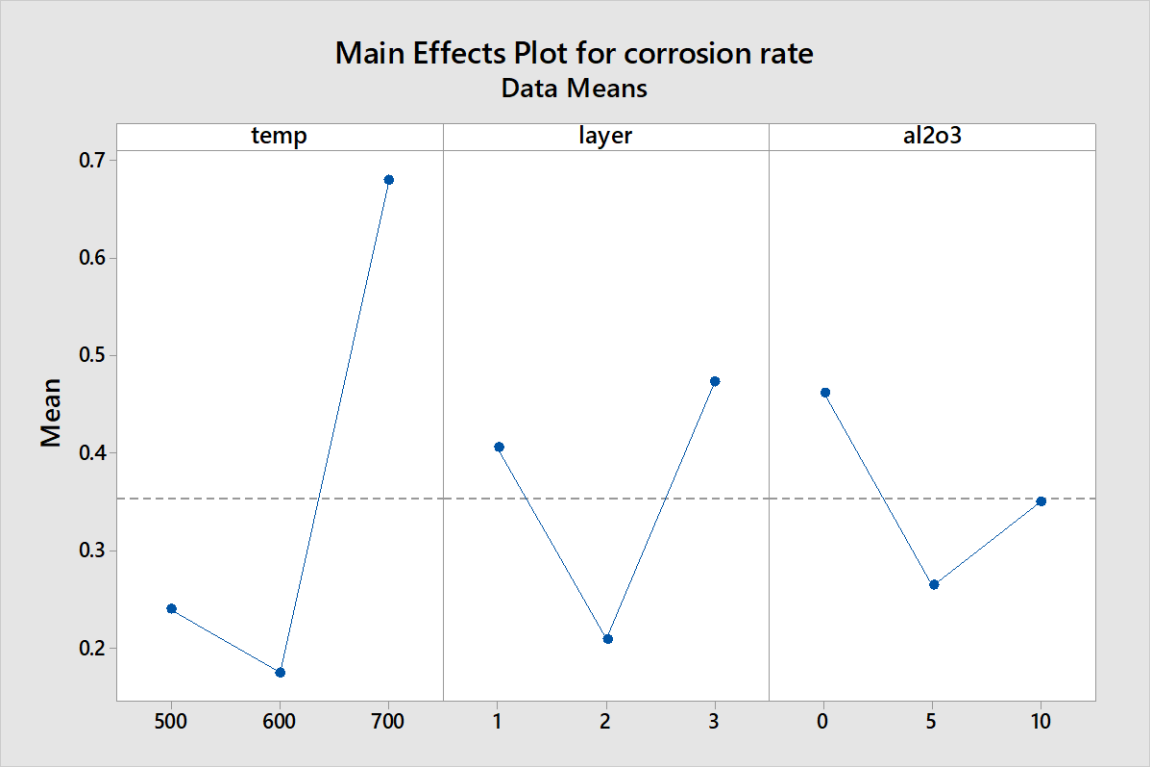

Figure (4.7) The effects of temperature, alumina content, and a number of layers on corrosion.

Table (4.6): ANOVA Results for corrosion rat

Source	Sum of Squares	df	Mean Square	F-value	p-value
Model	0.9986	9	0.1110	70.57	< 0.0001
A-Temperature	0.4822	1	0.4822	306.69	< 0.0001
B-no. of layer	0.0116	1	0.0116	7.37	0.0349
C-AL2O3	0.0311	1	0.0311	19.77	0.0043
AB	0.1124	1	0.1124	71.49	0.0001
AC	0.0102	1	0.0102	6.49	0.0437
BC	0.0004	1	0.0004	0.2594	0.6287
A^2	0.1471	1	0.1471	93.54	< 0.0001
B^2	0.0469	1	0.0469	29.82	0.0016
C^2	0.0024	1	0.0024	1.51	0.2651
Residual	0.0094	6	0.0016		
Cor Total	1.01	15			

4.2.7. Erosion- Corrosion test

table (4.3) shows the values of corrosion rates in the (Erosion-Corrosion) test in the center of concentrated sulfuric acid under flow conditions and a temperature of (65)°C to show the extent of the effect of the samples under examination on the effect of acid flow depending on the amount of weight loss during the area exposed to the acid in a time of (30) days of each model and extracting the erosion rate of the models during one day. The results showed a clear difference between the values of the corrosion rate samples coated with the base metal, equal to its value of 0.44 (g / cm². Day). The findings demonstrated that heat treatment directly impacted the erosion-corrosion rate. The Corrosion value varied from $7.5*15^{-5}$ to $22 *15^{-5}$ when the temperature was 500 C; the erosion rate ranged from $2.5*15^{-5}$ to $13*15^{-5}$ when the temperature was 600 C, and it went from 28 to 40 when the temperature was 700 C. This suggests that 600 C is the ideal temperature. According to the findings of the morphological analysis, the presence of surface flaws is directly related to the number of layers present in the structure. This is because a rise in the number of layers causes an increase in the production of numerous surface flaws, which in turn causes an increase in the corrosion rate caused by the influence of corrosive acid on the base metal. It was also discovered that raising the proportion of alumina from 0 to 10 had a discernible effect on the material's resistance to corrosion brought on by corrosion. This is because alumina significantly impacts surface flaws; increasing its concentration results in a higher density of the coating, which in turn decreases the number of surface flaws. The ANOVA table shows that temperature has the most significant effect, as its contribution ratio is 70.3 %. As a result, cracks form when the temperature increases, which leads to acid reaching the base metal. The results also showed that the effect of the number of layers is 11%, and for the same reason explained above,

increasing the number of layers to the 3 layers leads to the appearance of the number of surface defects. It was also noticed that alumina had a more negligible effect, as it was affected by 3.66%.

Table (4.7): ANOVA Results for Erosion – Corrosion

Source	Sum of Squares	df	Mean Square	F-value	p-value
Model	2.491E-07	9	2.768E-08	66.14	< 0.0001
A-Temperature	1.113E-07	1	1.113E-07	265.94	< 0.0001
B-no. of layer	1.690E-09	1	1.690E-09	4.04	0.0912
C-AL2O3	1.061E-09	1	1.061E-09	2.53	0.1625
AB	1.051E-08	1	1.051E-08	25.12	0.0024
AC	6.125E-10	1	6.125E-10	1.46	0.2719
BC	1.012E-09	1	1.012E-09	2.42	0.1709
A^2	4.546E-08	1	4.546E-08	108.63	< 0.0001
B^2	1.437E-08	1	1.437E-08	34.33	0.0011
C^2	7.459E-11	1	7.459E-11	0.1782	0.6876
Residual	2.511E-09	6	4.185E-10		
Cor Total	2.517E-07	15			

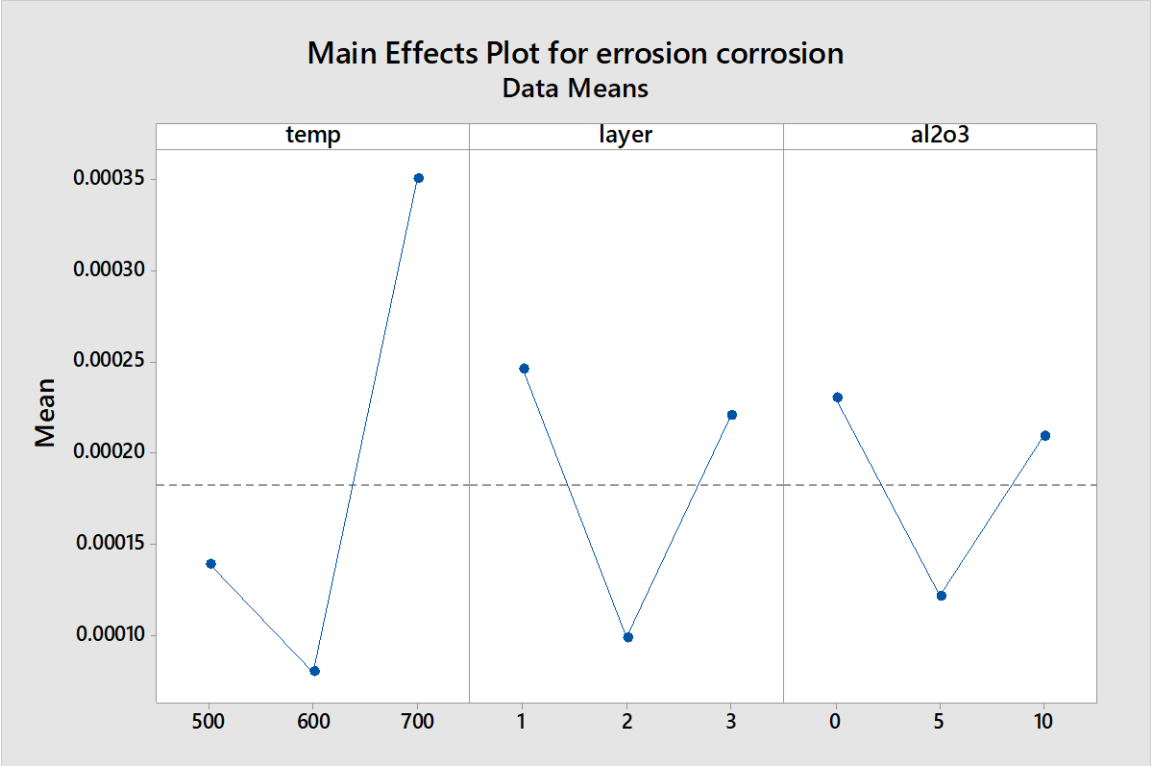

Figure (4.8) The effects of temperature, alumina content, and a number of layers on Erosion – Corrosion.

4.2.7. contact angle

Figure (4.9) shows the contact angles of all the films prepared in various ratios and for all angles. This figure is worth noting the difference in the value of the wetting angle, according to table (4.3) and figure (4.8). The correlation of the wetting angle with the corrosion current density[94], whereby an increase in the wetting angle leads to a decrease in the corrosion current density. This angle is brought to mind by a slight drop placed on a horizontal metal surface. The Young's relationship determines the shape of the drop. It is noted that the wetting angle for samples with a single layer is 82-117.1, and for samples, with two layers, it is 81.3-118.5, and for models with three layers, it is 75-90.8. The higher wetting behaviour in the S12, S11, S6, S7, and S4 samples could be related to their lower surface roughness, which indicates that the contact area of the H_2SO_4 solution to the surface of these samples is quiet low. This observation stands in good agreement with the corrosion resistance results, as the lower contact area reduces the ion release and corrosion effectivity of H_2SO_4 to the coated surface.

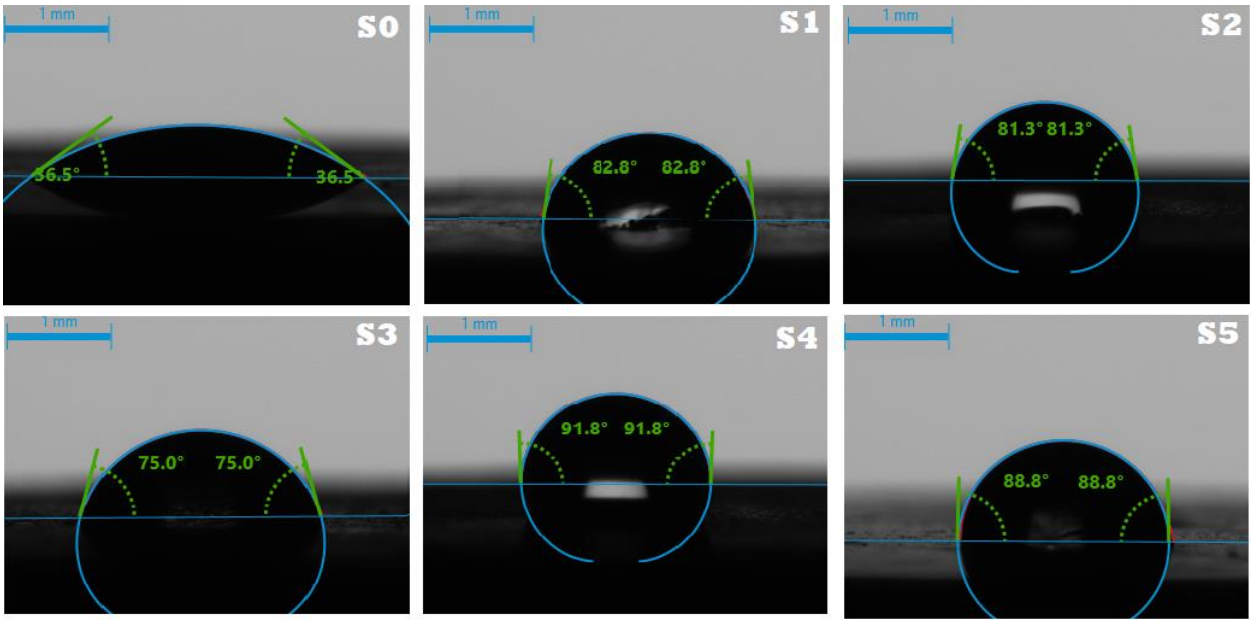

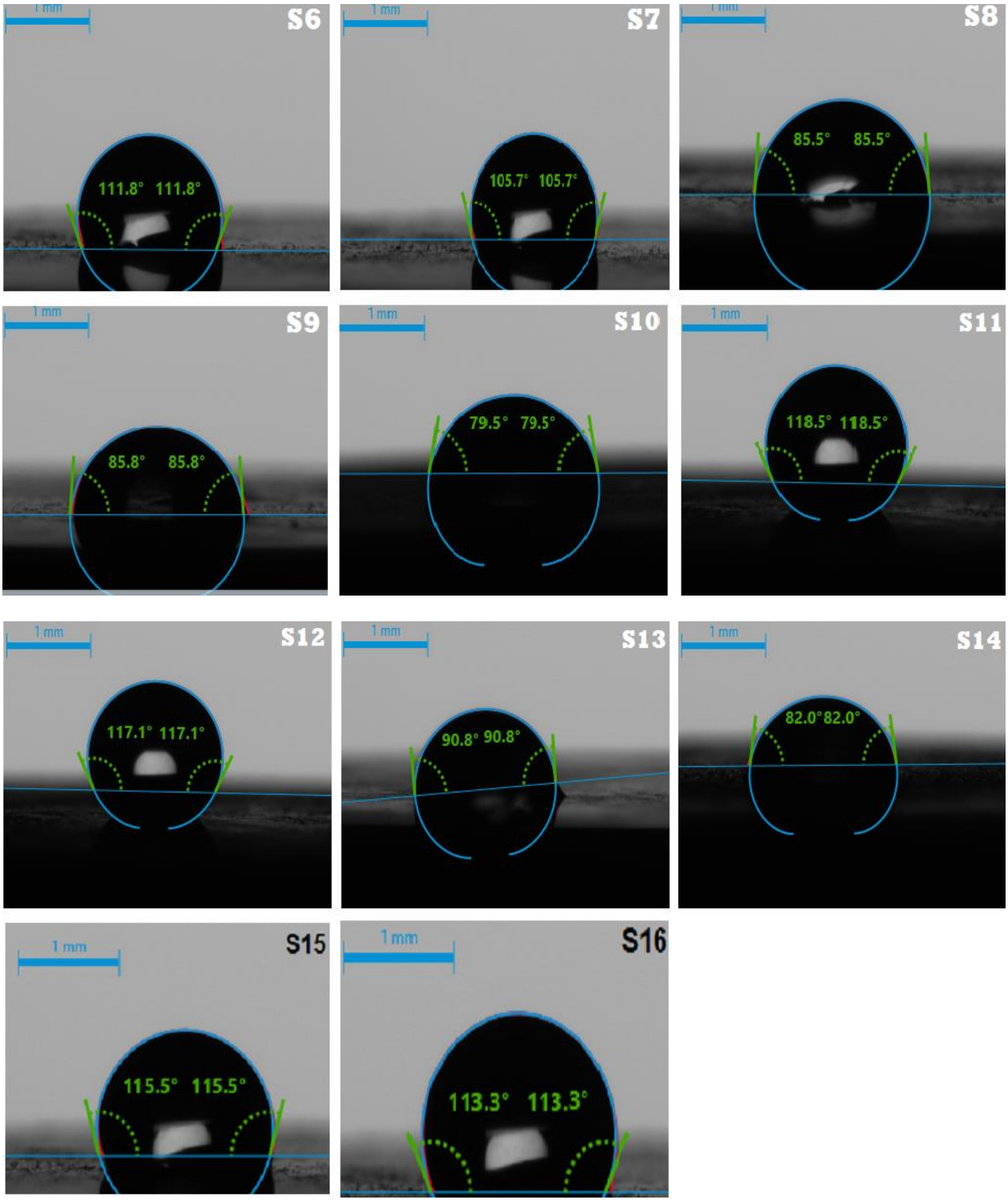

Figure (4.9): show a contact angle of all sample

4.3. Mathematical model

The correlation between treatment coefficients and responses was modeled with the help of a quadratic regression model. In equations (1), (2) , (3) and (4), the models and their determination coefficients with respect to annealing temperature, number of layers and percentage of additional alumina are provided, respectively. In order to predict the values of hardness, adhesion, optimum corrosion, and erosion

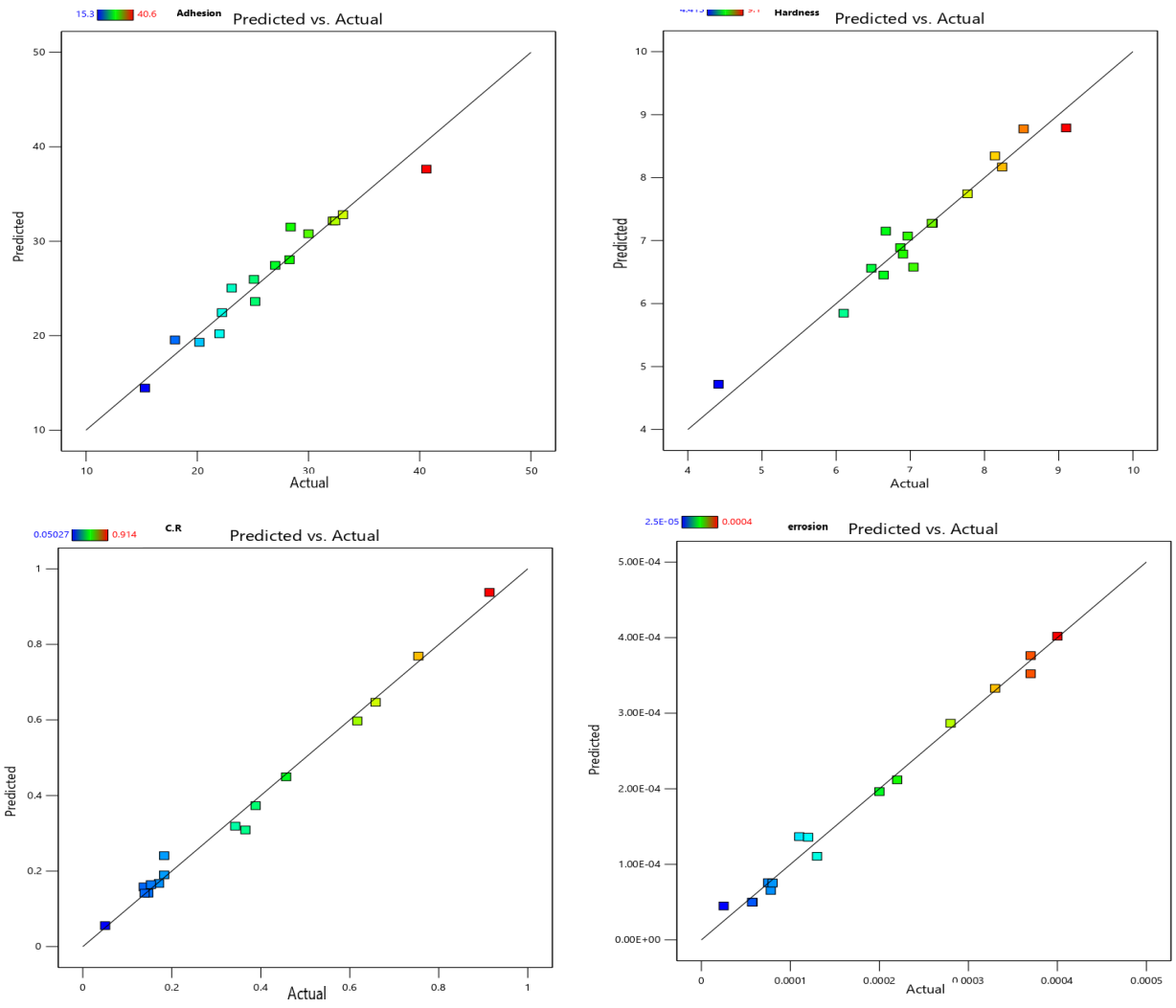

Figure 4.10. Actual versus Predicted plot: (A) hardness level, (B) adhesion,(C) corrosion rate, (D) erosion-corrosion.

1- Adhesion strength = 32.153103-2.418* A -3.066*B + 2.684*C - 9.48375*A^2

R^2 = 94.5 %

2- hardness = 7.2601875+ 0.8036* A 0.2857*B + 0.9456*C

R^2 = 95.13%

3- Corrosion Rate = 0.146 + 0.2195885 * A + 0.0340465 * B -0.055754 * C + 0.118534375 * AB -0.035703125 * AC + 0.2366403125 * A^2 + 0.1338153125 * B^2

R^2 = 99.06 %

4- Erosion Rate = 4.3875e-05 + 0.0001055 * A - 1.3e-05 * B - 1.03e-05 * C + 3.625e-05 * AB + 0.000133625 * A^2 + 7.6125e-05 * B^2

R^2 = 98.9 %

The above models can predict of hardness, adhesion, corrosion rate, and erosion-corrosion for any collection of temperature level , the number of layers, and the percentage of alumina. The mismatch between the findings that were expected based on these models and the actual data is demonstrated in figure (4.11). This figure demonstrates that mathematical models can able to reflect the answers within the confines of the experimental domain that has been specified.

4.4 Optimization

To find the optimum combination of input parameter combinations that provide the most acceptable compromise between several responses, the desirability function method was used to optimize the multiple response. The goal

of the optimization is to maximize both measures of hardness and adhesion and to reduce both measures of the rate of corrosion and erosion. The optimization results showed that the optimum coating layer to resist sulfuric acid is When the calcination temperature is about 588 °C, and it is a two-layer. The percentage of alumina is about 10 %. These set of parameters could produce a coating layer with the adhesion of 32.9 MPa and hardness of 8.25 GPa, and corrosion rate of 0.0373 mm y-1 and erosion-corrosion $3.45*10^{-5}$(g/cm^2.day) with the desirability of 0.864 as shown in figure (4.12)

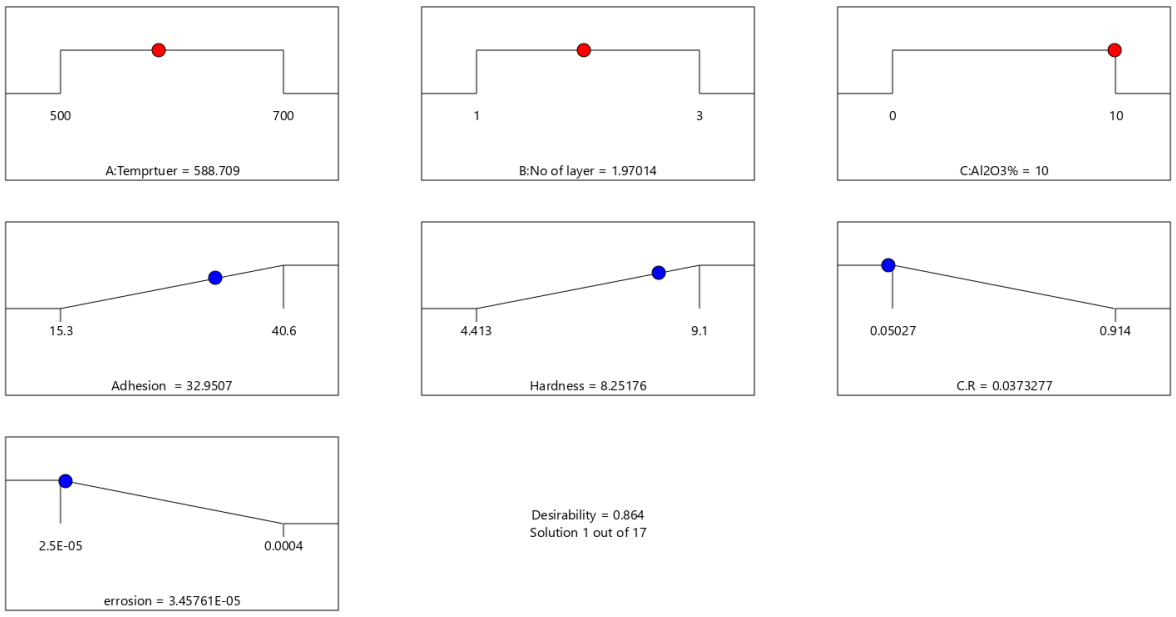

Figure 4.11. Actual versus Predicted plot: hardness level, adhesion corrosion rate, erosion-corrosion, and thickness.

4.5. Confirmation of the Optimum Results

The experimental confirmation is a crucial stage in the process of determining whether or not the optimization findings are reliable. The confirmation was carried out by experimentally applying the optimal production settings, and the results were compared to those that were anticipated in terms of the error

percentage (see table 4.8 for more information). The mistake rates reached such percentages. Confirmed to be within the allowed limits, with a maximum error percentage of 6 percent, which validates the correctness of the mathematical models to anticipate the replies, as well as confirmation of the response optimizer's effectiveness in choosing the best responses.

Table 4.8. Confirmation test.

Parameters	Predicted	Experiment	Error %
Adhesion	32.9	30.6	5.18%
Corrosion rate	0.039	0.038	2.6%
Erosion-corrosion	$3.5*10^{-5}$	$3.37*10^{-5}$	5%
Hardness	8.2	8.3	3%

Some physical and structural properties such as roughness (AFM), microstructure, and X-ray diffraction (XRD) analysis were performed on the sample with optimal properties.

4.5.1 A. X-Ray Diffraction (XRD) Analysis

The figure displays the XRD results for the TiO2 Nanopowder generated using the Sol-Gel method (4.12). The peaks are shown at the 2θ value range, and the diffraction peak at 2θ with 25.3 º, 38.3 º, 48 º, 54 º, and 62 º fits the crystal planes of the substance (101), (004), (200), (105), and (204), in that order, each of which points to the formation of anatase the Phase of Titanium Dioxide. The peaks in the graph are quite consistent with one another. The geographic position of When compared to the values found in the literature, the peaks reveal the presence of titanium dioxide [95].

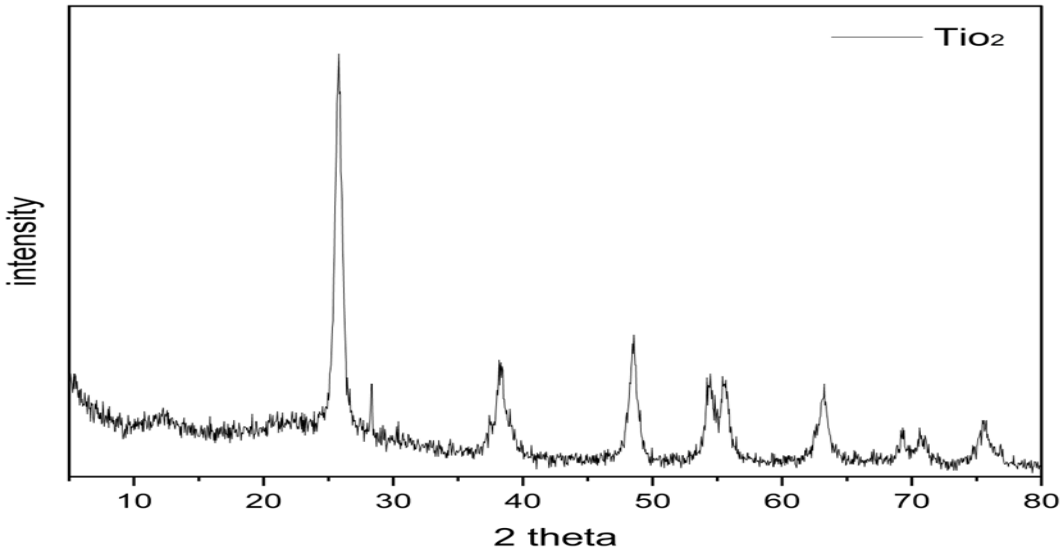

Figure (4.12): XRD patterns of TiO_2-based coating

4.5.2 AFM test and SEM test

The results of the acquired AFM are shown in Figure (13), where it can be seen that the surface roughness value is as low as 1.208nm , indicating the uniform of the coating layer. These results are also compatible with the results of the SEM test and with earlier research[87]. Figure (13) shows the obtained SEM results, where it is noted that the surface morphology is a homogeneous layer free of defectsthis ; indicates the efficiency of the coating layer.

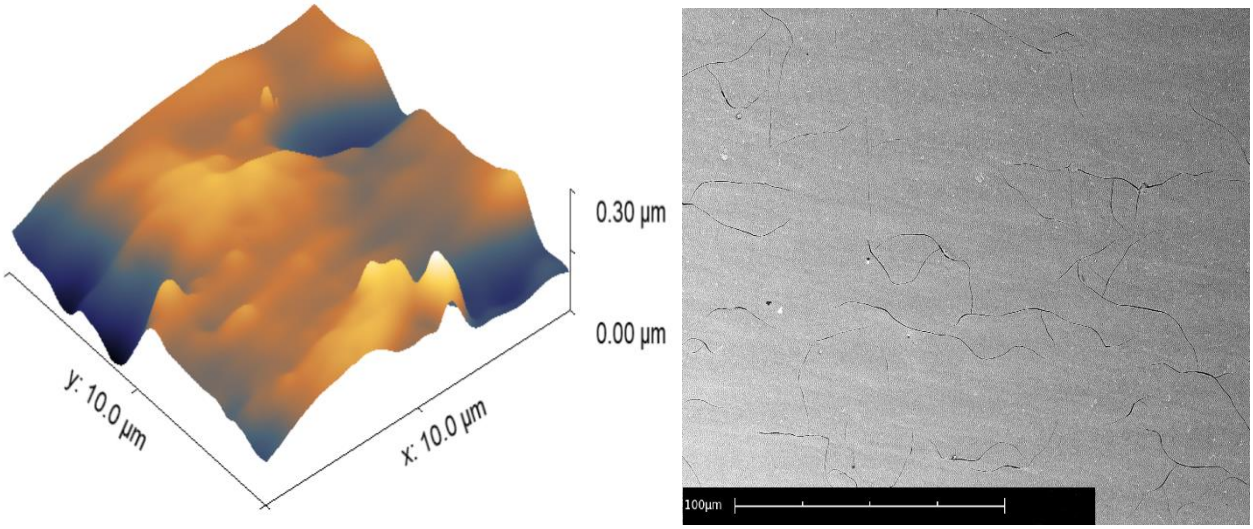

Figure (4.13): three-dimensional AFM images of the TiO_2–10 wt.% Al_2O_3 nanocomposite film with 2 layers thicknesses, SEM image of TiO_2-Al_2O_3 surface morphology.

Chapter

5

Conclusions and Recommendations

Chapter Five

Conclusions & Recommendations

5.1 Introduction

The conclusions drawn from this investigation are presented in this chapter. Additionally, it offers recommendations for further study that could be beneficial.

5-2 Conclusions

The following conclusions are drawn from this work: -

1- The sol-gel process, which is helped along by the production of TiO_2 (anatase) and Al_2O_3 Nanoparticles

2- It was possible to synthesize the transparent TiO_2-Al_2O_3 nanocomposite coatings at 600oC for 2 hours and 5°C/min using an appropriate thermal schedule.

3- According to the results of the XRD investigation, the alumina coating exhibits an amorphous structure.

4- Given that the erosion-corrosion of coated samples in the H_2SO_4 solution was better and that the variations of potential with time for coated samples were better, we can conclude that this coat offers carbon steel in this solution a high level of protection.

5-3 Suggestions for Future works

1- Adding additional elements to the coating, such as benzotriazole, to produce a composite of three different materials and analyze the corrosion behavior of carbon steel.

2. Investigating the effects of adding different ratios of (Al_2O_3) on the corrosion behavior.

3- Using another technique of coating method .

References

[1] S. . Tukur, M. M. Usman, I. Muhammad, and N. A. Sulaiman, “Effect of Tempering Temperature on Mechanical Properties of Medium Carbon Steel,” *Int. J. Eng. Trends Technol.*, vol. 9, no. 15, pp. 798–800, Mar. 2014, doi: 10.14445/22315381/IJETT-V9P350.

[2] J. K. Saha, “Corrosion of constructional steels in marine and industrial environment : frontier work in atmospheric corrosion.,” *Springer Sci. Bus. Media*, , 2013.

[3] Maysaa Muwafaq Abdulateef, “Enhancing the Fatigue Limit by Carburation and Shot Peening for Low Carbon Steel (AISI 1010)",” *Mater. Eng. Dep. 2015.*,

[4] D. E. J. Talbot and J. D. R. Talbot, “Corrosion science and technology,” *Choice Rev. Online*, vol. 45, no. 04, pp. 4, 2007, doi: 10.5860/choice.45-2055.

[5] Dariva Koch, P. H. Brogers “Single-desirability based - Taguchi approach that the optimal parameters for microhardness”.

[6] R. Singh *et al.*, “CORROSION CONTROL FOR OFFSHORE STRUCTURES Cathodic Protection and High-Efficiency Coating First edition,” 2014.

[7] D. Wang and G. P. Bierwagen, “Sol-gel coatings on metals for corrosion protection,” *Progress in Organic Coatings*, vol. 64, no. 4. pp. 327–338, Mar. 2009. doi: 10.1016/j.porgcoat.2008.08.010.

[8] E. C. L. Mancini L. H., “"Nanocomposites : preparation, properties and performance, book” *Chp.4,* , 2008.

[9] J. Jordan, K. I. Jacob, R. Tannenbaum, M. A. Sharaf, and I. Jasiuk, “Experimental trends in polymer nanocomposites - A review,” *Materials Science and Engineering A*, vol. 393, no. 1–2. pp. 1–11, Feb. 25, 2005. doi: 10.1016/j.msea.2004.09.044.

[10] T. A. N. P. C. and C. N. X. P. N.Tri, “Nanocomposite Coatings:Preparation, Characterization, Properties, and Applications,” *Int. J. Corros.* , 2018.

[11] P. Geethamani and P. K. Kasthuri, “The inhibitory action of expired asthalin drug on the corrosion of mild steel in acidic media: A comparative study,” *J. Taiwan Inst. Chem. Eng.*, vol. 63, pp. 490–499, 2016, doi: 10.1016/j.jtice.2016.03.008.

[12] M. F. Montemor, “Functional and smart coatings for corrosion protection: A review of recent advances,” *Surf. Coatings Technol.*, vol. 258, pp. 17–37, 2014, doi: 10.1016/j.surfcoat.2014.06.031.

[13] *Am. J. Eng. Res.* “Sol-gel coatings" American Journal of Engineering Research (AJER) 2008,

[14] J. R. Davis, “Corrosion Understanding the Basics‘‘,.” 2000.

[15] G. H. Koch, P. H. Brogers, N. Thompson, Y. P. Virmani, and J. H. Payer, “Corrosion Cost and Preventive Strategies in the United States, Corrosion Cost and Preventive Strategies in the United States, FHWA Report; FHWA-RD-01–156,” p. 2002, ,

[16] C.G. Dariva and A. F. Galio, “Corrosion Inhibitors – Principles, Mechanisms and Applications”Boakye, Osei Ernest,” *Implement. Sci.*, vol. 39, no. 1, pp. 1–24, 2014,

[17] S. E. Nataraja, T. V. Venkatesha, and H. C. Tandon, “Computational and experimental evaluation of the acid corrosion inhibition of steel by tacrine,” *Corros. Sci.*, vol. 60, pp. 214–223, 2012, doi: 10.1016/j.corsci.2012.03.034.

[18] M. W. Kendig and R. G. Buchheit, “Corrosion inhibition of aluminum and aluminum alloys by soluble chromates, chromate coatings, and chromate-free coatings,” *Corrosion*, vol. 59, no. 5, pp. 379–400, 2003, doi: 10.5006/1.3277570.

[19] Z. Panossian, N. L. de Almeida, R. M. F. de Sousa, G. de S. Pimenta, and L. B. S. Marques, “Corrosion of carbon steel pipes and tanks by concentrated sulfuric acid: A review,” *Corros. Sci.*, vol. 58, pp. 1–11, 2012, doi: 10.1016/j.corsci.2012.01.025.

[20] F. Ferrer, T. Faure, J. Goudiakas, and E. Andrés, “Acoustic emission study of active-passive transitions during carbon steel erosion-corrosion in concentrated sulfuric acid,” *Corros. Sci.*, vol. 44, no. 7, pp. 1529–1540, 2002, doi: 10.1016/S0010-938X(01)00148-2.

[21] B. Bobić, S. Mitrović, M. Babić, and I. Bobić, “Corrosion of Metal-Matrix composites with aluminium alloy substrate,” *Tribol. Ind.*, vol. 32, no. 1, pp. 3–11, 2010.

[22] C. Verma, M. A. Quraishi, K. Kluza, M. Makowska-Janusik, L. O. Olasunkanmi, and E. E. Ebenso, “Corrosion inhibition of mild steel in 1M HCl by D-glucose derivatives of dihydropyrido

[23] Jayanta Kumar Saha Corrosion of Constructional Steels in Marine and Industrial Environment Frontier Work in Atmospheric Corrosion springer, 2013.,”

[24] J. Alcántara, D. de la Fuente, B. Chico, J. Simancas, I. Díaz, and M. Morcillo, "Marine atmospheric corrosion of carbon steel: A review," *Materials (Basel).*, vol. 10, no. 4, 2017, doi: 10.3390/ma10040406.

[25] D. H. Abdeen, M. El Hachach, M. Koc, and M. A. Atieh, "A review on the corrosion behaviour of nanocoatings on metallic substrates," *Materials (Basel).*, vol. 12, no. 2, 2019, doi: 10.3390/ma12020210.

[26] - W. F. Gale, T. C. Totemeier," Smithells metals reference book", Butterworth-Heinemann" 2008,

[27] "-W. F. Gale, S. Vivekanandan," Smithells metals reference book", 8," p. 2004,

[28] "P. A. Schweitzer, 'Corrosion Engineering 3 Volume Set,' Marcel Dekker, Inc., New York, .," p. 1996,.

[29] - R. Baboian," Corrosion tests and standards, application and interpretation", ASTM International, 2," p. 2005,.

[30] Strehblow, H. H., & Marcus, P. (2011). Fundamentals of corrosion. In Corrosion Mechanisms in Theory and Practice: Third Edition," p. 2011,

[31] S. S. Rajahram, T. J. Harvey, and R. J. K. Wood, "Erosion-corrosion resistance of engineering materials in various test conditions," *Wear*, vol. 267, no. 1–4, pp. 244–254, 2009,

[32] K. Sasaki and G. T. Burstein, "Observation of a threshold impact energy required to cause passive film rupture during slurry erosion of stainless steel," *Philos. Mag. Lett.*, vol. 80, no. 7, pp.

[33] A. S. H. Makhlouf, V. Herrera, and E. Muñoz, *Corrosion and protection of*

the metallic structures in the petroleum industry due to corrosion and the techniques for protection. Elsevier Ltd, 2018..

[34] T. J. Ross, *FUZZY LOGIC WITH ENGINEERING Second Edition*. 2004.

[35] P. R. Roberge, *Handbook of corrosion engineering*, vol. 37, no. 09. 2000. doi: 10.5860/choice.37-5122.

[36] A. Popoola, O. Olorunniwo, and O. Ige, "Corrosion Resistance Through the Application of Anti- Corrosion Coatings," *Dev. Corros. Prot.*, p. 57420, 2014, doi: 10.5772/57420.

[37] D. Dwivedi, K. Lepková, and T. Becker, "Carbon steel corrosion: a review of key surface properties and characterization methods," *RSC Adv.*, vol. 7, no. 8, pp. 4580–4610, 2017, doi: 10.1039/C6RA25094G.

[38] R. Javaherdashti, "How corrosion affects industry and life," *Anti-Corrosion Methods Mater.*, vol. 47, no. 1, pp. 30–34, 2000, doi: 10.1108/00035590010310003.

[39] E. Shekari, F. Khan, and S. Ahmed, "Economic risk analysis of pitting corrosion in process facilities," *Int. J. Press. Vessel. Pip.*, vol. 157, pp. 51–62, 2017, doi: 10.1016/j.ijpvp.2017.08.005.

[40] R. Singh, D. M. Liu *CORROSION CONTROL FOR OFFSHORE STRUCTURES CORROSION CONTROL FOR Cathodic Protection and*. 2014.

[41] S. Sovilj-Nikić, B. Sovilj, G. Varga, N. Ungureanu, and V. Blanuša, "Analysis of the tool life of coated hob milling tools for gear cutting of cylindrical gear," *MATEC Web Conf.*, vol. 184, 2018, doi:

10.1051/matecconf/201818403011.

[42] X. Wang and X. Chen, “Novel nanomaterials for biomedical, environmental and energy applications,” *Nov. Nanomater. Biomed. Environ. Energy Appl.*, pp. 1–493, 2018, doi: 10.1016/C2017-0-01068-6.

[43] Schaefer, fak. Mathematik and Physik ., ‘Nanocrystalline materials’; Springer, Berlin, Heidelberg, 2010,” p. 2010,

[44] X. Wang *et al.*, “Fabrication and corrosion resistance of calcium phosphate glass-ceramic coated Mg alloy via a PEG assisted sol-gel method,” *Ceram. Int.*, vol. 40, no. 2, pp. 3389–3398, 2014, doi: 10.1016/j.ceramint.2013.09.093.

[45] D. M. Liu, Q. Yang, and T. Troczynski, “Sol-gel hydroxyapatite coatings on stainless steel substrates,” *Biomaterials*, vol. 23, no. 3, pp. 691–698, 2002, doi: 10.1016/S0142-9612(01)00157-0.

[46] K. Y. Hung, S. C. Lo, C. S. Shih, Y. C. Yang, H. P. Feng, and Y. C. Lin, “Titanium surface modified by hydroxyapatite coating for dental implants,” *Surf. Coatings Technol.*, vol. 231, pp. 337–345, 2013, doi: 10.1016/j.surfcoat.2012.03.037.

[47] A. Tahmasbi Rad, M. Solati-Hashjin, N. A. A. Osman, and S. Faghihi, “Improved bio-physical performance of hydroxyapatite coatings obtained by electrophoretic deposition at dynamic voltage,” *Ceram. Int.*, vol. 40, no. 8 PART B, pp. 12681–12691, 2014, doi: 10.1016/j.ceramint.2014.04.116.

[48] R. S. (Gaurav Bahuguna, Amit Kumar, “Thin film coating through sol-gel Technique”, Chemical sciences,” vol. 6, p. 2016,

[49] “Lee B., Sridhar K., ‘Chemical processing of ceramics’, Chp.6, pp.275, 2,” p. 2005,

[50] K. D. Sattler, “, ‘Handbook of Nanophysics: Nanoparticles and Quantum Dots’ Chp.1, pp.1 , Taylor and Francis Group, LLC, 2011,”

[51] E. Turova, N., Turevskaya, “‘The Chemistry of metal alkoxides’, Kluwer Academic Publishers, Boston, 2002,”

[52] N. P. Markus N., .“, ‘Metal oxide nanoparticles in organic solvents’, Springer, 2009,” p..

[53] R. M. N., “‘ Ceramic processing and sintering’, Chp.5, pp.248, Marcel Dekker, Inc ,2003,”.

[54] S. Mahshid, M. Askari, and M. S. Ghamsari, “Synthesis of TiO2 nanoparticles by hydrolysis and peptization of titanium isopropoxide solution,” *J. Mater. Process. Technol.*, vol. 189, no. 1–3, pp. 296–300, 2007, doi: 10.1016/j.jmatprotec.2007.01.040.

[55] and M. B. F.A. Cotton, G. Wilkinson, C.A. Murillo, “Advanced Inorganic Chemistry". John Wiley & Sons,p. 180-223 1999,” p. 1999, 1999.

[56] R. Lach, K. Haberko, M. M. Bućko, M. Szumera, and G. Grabowski, “Ceramic matrix composites in the alumina/5-30vol.% YAG system,” *J. Eur. Ceram. Soc.*, vol. 31, no. 10, pp. 1889–1895, 2011, doi: 10.1016/j.jeurceramsoc.2011.04.003.

[57] A. A. Tsyganenko and P. P. Mardilovich, “Structure of alumina surfaces,” *J. Chem. Soc. - Faraday Trans.*, vol. 92, no. 23, pp. 4843–4852, 1996, doi: 10.1039/ft9969204843.

[58] P. P. Askeland, D. R., and Phule, "′, '"The science and engineering of materials"', 4," p. 2003,

[59] "B. Tan, 'Controlled synthesis and functionalization of nanoporous solgel silica particles and gels', Ph.D. Thesis, University of Kentucky, Chp.1, 2005.

[60] R. Vijayalakshmi and K. V Rajendran, "Synthesis of Nano-TiO 2 by Sol-Gel Route : Effect of Solvent and Temperature on the Optical Properties," vol. 7, no. 1, pp. 105–115, 2011.

[61] mohamed n . rahaman, "sintering of ceramics." 2020,

[62] Taylor & Francis Group, *Nanomaterials: Synthesis, Properties and Applications*.book 1996.

[63] N. A. J. M. S. ByJohn D. Wright, "Sol-Gel Materials Chemistry and Applications," 2000.

[64] J.Serb.Chem.Soc., (Organic Chemistry and Biochemistry) 2001

[65] S. Doeuff, M. Henry, C. Sanchez, and J. Livage, "The gel route to Cr3+-doped TiO2, an ESR study," *J. Non. Cryst. Solids*, vol. 89, no. 1–2, pp. 84–97, 1987, doi: 10.1016/S0022-3093(87)80323-X.

[66] R. Hiesgen and K. A. Friedrich, "Atomic force microscopy," *PEM Fuel Cell Diagnostic Tools*, pp. 395–421, 2011, doi: 10.4011/shikizai.93.321.

[67] L. E. Scriven, "Dip Coating and Spin Coating," *MRS Proc.*, vol. 121, no. May, pp. 717–729, 1988.

[68] D. A. H. Hanaor, G. Triani, and C. C. Sorrell, "Morphology and photocatalytic activity of highly oriented mixed phase titanium dioxide thin films," *Surf. Coatings Technol.*, vol. 205, no. 12, pp. 3658–3664, 2011, doi:

10.1016/j.surfcoat.2011.01.007.

[69] P. C. Sukanek, “Spin Coating.,” *J. imaging Technol.*, vol. 11, no. 4, pp. 184–190, 1985, doi: 10.1201/9781315108292-33.

[70] D. Grosso, “How to exploit the full potential of the dip-coating process to better control film formation,” *J. Mater. Chem.*, vol. 21, no. 43, pp. 17033–17038, 2011, doi: 10.1039/c1jm12837j.

[71] I. John Wiley & Sons, “Organic Coatings,” *Sci. Technol.*, vol. 9, no. 2, p. 10, 2007, [Online].

[72] R. Flink, ‘ Industrial Coating of Metal Surfaces’, Tikkurila Oyj, 2nd Edition, Ch.6, pp. 28-33, 2011.,” p. 2011, 2011.

[73] J. Antoy, *Design of Experiments for Engineers and Scientists: Second Edition*. 2014. doi: 10.1016/C2012-0-03558-2.

[74] S. Sathish and S. Vivekanandan, “Parametric optimization for floating drum anaerobic bio-digester using Response Surface Methodology and Artificial Neural Network,” *Alexandria Eng. J.*, vol. 55, no. 4, pp. 3297–3307, Dec. 2016, doi: 10.1016/j.aej.2016.08.010.

[75] S. J. M. Breig and K. J. K. Luti, “Response surface methodology: A review on its applications and challenges in microbial cultures,” in *Materials Today: Proceedings*, 2021, vol. 42, pp. 2277–2284. doi: 10.1016/j.matpr.2020.12.316.

[76] S. A. Oliaee and S. Naghibi, “Anticorrosion assessment of Al2O3-TiO2 composite thin films derived from sol-gel dipping technique,” *Int. J. Appl. Ceram. Technol.*, vol. 15, no. 3, pp. 689–700, May 2018, doi:

10.1111/ijac.12849.

[77] H. Vaghari, Z. Sadeghian, and M. Shahmiri, “Investigation on synthesis, characterisation and electrochemical properties of TiO2-Al2O3 nanocomposite thin film coated on 316L stainless steel,” *Surf. Coatings Technol.*, vol. 205, no. 23–24, pp. 5414–5421, 2011, doi: 10.1016/j.surfcoat.2011.06.004.

[78] M. S. Sharifiyan, A. Shanaghi, H. Moradi, and P. K. Chu, “Effects of high concentration of Benzotriazole on corrosion behavior of nanostructured titania-alumina composite coating deposited on Al 2024 by sol-gel method,” *Surf. Coatings Technol.*, vol. 321, pp. 36–44, Jul. 2017, doi: 10.1016/j.surfcoat.2017.04.041.

[79] E. Celik, I. Keskin, I. Kayatekin, F. Ak Azem, and E. Özkan, “Al2O3-TiO2 thin films on glass substrate by sol-gel technique,” *Mater. Charact.*, vol. 58, no. 4, pp. 349–357, Apr. 2007, doi: 10.1016/j.matchar.2006.05.015.

[80] A. R. Simbar, A. Shanaghi, H. Moradi, and P. K. Chu, “Corrosion behavior of functionally graded and self-healing nanostructured TiO2–Al2O3 - Benzotriazole coatings deposited on AA 2024-T3 by the sol-gel method,” *Mater. Chem. Phys.*, vol. 240, no. June 2017, p. 122233, 2020, doi: 10.1016/j.matchemphys.2019.122233.

[81] A. Katoch, H. Kim, T. Hwang, and S. S. Kim, “Preparation of highly stable TiO 2 sols and nanocrystalline TiO 2 films via a low temperature sol-gel route,” *J. Sol-Gel Sci. Technol.*, vol. 61, no. 1, pp. 77–82, Jan. 2012, doi: 10.1007/s10971-011-2593-6.

[82] D. Chen and E. H. Jordan, “Sol-gel synthesis and characterization of Al2O 3-

TiO2 nanocrystalline powder," *J. Sol-Gel Sci. Technol.*, vol. 50, no. 1, pp. 44–47, Apr. 2009, doi: 10.1007/s10971-009-1897-2.

[83] A. Tiwari, "Nanomechanical Analysis of Hybrid Silicones and Hybrid Epoxy Coatings—A Brief Review," *Adv. Chem. Eng. Sci.*, vol. 02, no. 01, pp. 34–44, 2012, doi: 10.4236/aces.2012.21005.

[84] N. R. Ali, H. A. H. Al, and E. M. S. Salih, "The effect of adding Silicon Carbide microparticles to the optimum chromium plating on improving the corrosion resistance of carbon steel in concentrated sulfuric acid medium (98 %)," vol. 7, no. 1, pp. 4855–4869, 2022.

[85] V. Kumar, R. Shekhar, and K. Balani, "Corrosion Behavior of Novel Mg-9Li-7Al-1Sn and Mg-9Li-5Al-3Sn-1Zn Alloys in NaCl Aqueous Solution," *J. Mater. Eng. Perform.*, vol. 24, no. 10, pp. 4060–4070, Oct. 2015, doi: 10.1007/s11665-015-1687-7.

[86] R. T. Loto and C. A. Loto, "Potentiodynamic Polarization Behavior and Pitting Corrosion Analysis of 2101 Duplex and 301 Austenitic Stainless Steel in Sulfuric Acid Concentrations," *J. Fail. Anal. Prev.*, vol. 17, no. 4, pp. 672–679, Aug. 2017, doi: 10.1007/s11668-017-0291-6.

[87] H. Vaghari, Z. Sadeghian, and M. Shahmiri, "Investigation on synthesis, characterisation and electrochemical properties of TiO2-Al2O3 nanocomposite thin film coated on 316L stainless steel," *Surf. Coatings Technol.*, vol. 205, no. 23–24, pp. 5414–5421, Sep. 2011, doi: 10.1016/j.surfcoat.2011.06.004.

[88] U. O. Akkaya Arier and F. Z. Tepehan, "Influence of Al2O3:TiO2 ratio on the structural and optical properties of TiO2-Al2O3 nano-composite films

produced by sol gel method," *Compos. Part B Eng.*, vol. 58, pp. 147–151, 2014, doi: 10.1016/j.compositesb.2013.10.023.

[89] S. R. Barbato, J. F. Ponce, M. L. Jara, J. S. Cuevas, and R. A. Egaña, "STUDY OF THE EFFECT OF TEMPERATURE ON THE HARDNESS, GRAIN SIZE, AND YIELD IN ELECTRODEPOSITION OF CHROMIUM ON 1045 STEEL," 2008.

[90] Z. H. Wang, Y. X. Leng, N. Huang, and M. H. Zhu, "Adhesion Evaluation of Titanium Oxides Films on 316L Stainless Steel Substrate," *Key Eng. Mater.*, vol. 353–358, pp. 2127–2130, 2007,

[91] Y. X. Leng, J. Wang, P. Yang, J. Y. Chen, and N. Huang, "The adhesion and clinical application of titanium oxide film on a 316 L vascular stent," *Surf. Coatings Technol.*, vol. 363, no. November, pp. 430–435, 2019, doi: 10.1016/j.surfcoat.2018.12.021.

[92] R. Palanivelu and A. R. Kumar, "Scratch and wear behaviour of plasma sprayed nano ceramics bilayer Al 2 O 3 -13 wt%TiO 2 /hydroxyapatite coated on medical grade titanium substrates in SBF environment," *Appl. Surf. Sci.*, vol. 315, no. 1, pp. 372–379, 2014, doi: 10.1016/j.apsusc.2014.07.167.

[93] N. O. G zer, J. P. Cronin, Y.-J. Yao, and A. P. Tomsia, "Optical properties of sol}gel deposited Al O "lms." no. June 2017

[94] S. K. Behera, A. Kumar P, N. Dogra, M. Nosonovsky, and P. Rohatgi, "Effect of Microstructure on Contact Angle and Corrosion of Ductile Iron: Iron-Graphite Composite," *Langmuir*, vol. 35, no. 49, pp. 16120–16129, Dec. 2019, doi: 10.1021/acs.langmuir.9b02395.

[95] "Suresh Sagadevan" Synthesis and electrical properties of Ti02 nanoparticles

using a wet chemical technique" American Journal of Nanoscience and Nanotechnology.p.14, 2013.," p. 2013,

الخلاصة

من المعروف أن تطبيق الطلاءات على المعادن من أكثر الطرق فعالية لحماية المعدن من تأثيرات البيئة المحيطة.حيث تم استخدام أوكسيد التيتانيوم (TiO_2) وأوكسيد الألومنيوم (Al_2O_3) في هذه الدراسة نظرًا لخصائصهما الفريدة كمواد طلاء وتم تحضيرهما باستخدام تقنية Sol-Gel وطريقة Dip Coated. تم اجراء الطلاءات لحماية الأنابيب من حامض الكبريتيك المركز بنسبة (98٪). بلاضافه الى ذلك يعتمد الطلاء على تصميم التجارب من خلال نهج سطح الاستجابة (response surface) وكانت المتغيرات هي درجة الحرارة ، وعدد الطبقات المطبقة ، وكمية الألومينا المضافة هي العوامل الرئيسية التي تغيرت أثناء التجربة. كما تم التحقق من الاختبارات عن طريق حيود الأشعة السينية (XRD) ، والمسح المجهري الإلكتروني (SEM) ، والخشونة (AFM) ، واختبارات التآكل التي أجريت في وسط يحتوي على حامض بنسبة 98 ٪ كما تم اجراء فحص المجهر الضوئي . حيث يعتمد نجاح هذه الدراسة على إنشاء النموذج المثالي لأفضل معالجة حرارية وعدد الطبقات ونسبة إضافة الألومينا. تم اكتشاف من خلال تصميم التجارب أن افضل درجة حرارة هي 588C ، عدة طبقات تساوي 2 ، ونسبة إضافة الألومينا تساوي 10٪ أعطت أفضل النتائج فيما يتعلق بمقاومة الأحماض. وفقًا للنتائج ، زادت قيمة صلابة المادة من 2.1 الى 8.2 كيكا باسكال عند تعرضها لهذه الظروف ، وكانت قيمة قوة الالتصاق 32.8 ميجا باسكال عند قياسها بالضروف المثلى . بالإضافة إلى ذلك ، انخفضت قيمة معدل التآكل إلى $0.036\ mm\ y^{-1}$ ، وكان معدل التآكل بالتعريه $3.1 * 10^{-5}\ (g/cm^2.day)$. تم تحسين معدل التآكل وقيمة التآكل بالتعريه بنسبة 98٪ و 99٪. تم تخفيض كل من هذه القيم من قيمها الأصلية. وفقًا لنتائج اختبار التآكل ، فإن هذا الطلاء مناسب للاستخدام مع حامض الكبريتيك االمركز بنسبة 98%.

وزارة التعليم العالي والبحث العلمي
جامعـــــــــة بابـــــــــل
كليـــــــة هنـــــدسة المواد
قســـــم هنـــدسة المـــعادن

الامثليه المتعددة للطلاء بطريقة السول – جل لحماية الفولاذ واطئ الكاربون من التأكل

رسالة

مقدمة إلى قسم هندسة المعادن في كلية هندسة المواد / جامعة بابل وهي جزء من متطلبات نيل درجة الماجستير في

هندسة المواد/ المعادن

من قبل

عمار حسين علي حسين

(بكالوريوس هندسة مواد)

(2015)

بإشراف

أ. د. اقبال محمد سعيد صالح

أ. د. حيدر عبد الحسين الجبوري

2022 م **1442 هـ**